

THE EXTRAGALACTIC BACKGROUND LIGHT, THE HUBBLE CONSTANT, AND ANOMALIES: CONCLUSIONS FROM 20 YEARS OF TEV GAMMA-RAY OBSERVATIONS

J. BITEAU¹ & D. A. WILLIAMS²

Santa Cruz Institute for Particle Physics and Department of Physics,
 University of California at Santa Cruz, Santa Cruz, CA 95064, USA

To be submitted to Astrophysical Journal

ABSTRACT

Ground-based observatories have been collecting 0.2 – 20 TeV gamma rays from blazars for about twenty years. These gamma rays can experience absorption along the line of sight due to interactions with the extragalactic background light (EBL). In this paper, we show that the gamma-ray optical depth can be reduced to the convolution product of an EBL kernel with the EBL intensity, assuming a particular form for the EBL evolution. We extract the absorption signal from the most extensive set of TeV spectra from blazars collected so far and unveil a broad-band EBL spectrum from mid-ultraviolet to far infrared. This spectrum is in good agreement with the accumulated emission of galaxies, constraining unresolved populations of sources. We propose a data-driven estimate of the Hubble constant based on the comparison of local and gamma-ray measurements of the EBL. After setting stringent upper-limits on the redshift of four TeV blazars, we investigate the 106 gamma-ray spectra in our sample and find no significant evidence for anomalies. The intrinsic TeV spectra are not harder than their GeV counterpart, and no spectral upturn is visible at the highest optical depths. Finally, we investigate a modification of the pair-creation threshold due to Lorentz invariance violation. A mild excess prevents us from ruling out an effect at the Planck energy, and we constrain for the first time the energy scale of the modification to values larger than sixty percent of the Planck energy.

Subject headings: astroparticle physics, cosmology: observations, diffuse radiation, galaxies: active, gamma rays: galaxies

1. INTRODUCTION

The universe is not as dark as we sometimes imagine; even its largest voids are filled with light. The most intense of these photon fields, the cosmic microwave background (CMB), covers the millimeter wavelength range and carries the relic radiation that escaped the epoch of recombination, less than half a million years after the Big Bang. At lower wavelength, from 0.1 to 1000 μm , the universe is populated by the light that stars and galaxies have emitted since the epoch of reionization ($z \lesssim 10$). Part of the light initially radiated in the ultraviolet (UV) and optical (O) bands is directly observable in the cosmic optical background (COB, 0.1 – 8 μm). The rest was absorbed by dust in the interstellar medium and around active galactic nuclei (AGN) and was subsequently reradiated at lower energies, in the infrared (IR), forming the cosmic infrared background (CIB, 8 – 1000 μm). The sum of the COB and CIB, the extragalactic background light (EBL), thus carries the 13 billion years' radiation history of the universe and is a critical observable for models of reionization, galaxy formation and evolution, as well as high-energy-astrophysics phenomena, as we discuss.

The main constraints on the EBL from observations in the UV-O-IR come in two flavors: direct observations, which tend to be contaminated by bright foregrounds such as the zodiacal light, and estimates from integrated galaxy counts, which sum the light emitted by known populations of sources (e.g., Madau & Pozzetti 2000). The latter do not include contributions from truly dif-

fuse components or unobserved populations of sources, such as primordial stars (Pop. III) and miniquasars that could have initiated the reionization of the universe (e.g. Madau et al. 2004; Cooray & Yoshida 2004), or intra-halo light that was recently invoked to explain the near-IR anisotropies observed by CIBER (Zemcov et al. 2014).

Stringent constraints also come from observations of gamma rays, which are more energetic than the EBL photons by twelve orders of magnitude. The underlying process, described by Nikishov (1962) and Gould & Schröder (1967a,b), is the creation of electron-positron pairs in the interaction of gamma rays from extragalactic sources with the EBL photon field. The survival probability of a gamma ray, or gamma-ray absorption, is characterized by an exponential attenuation law, $\exp(-\tau)$, where the optical depth, τ , depends on the redshift of the source and on the gamma-ray energy.

The detection of the first distant gamma-ray sources led to the first observational constraints on gamma-ray absorption (Stecker et al. 1992). Extragalactic sources observed in gamma rays, e.g. by *Fermi*-LAT in the high-energy band (HE, 0.1 – 300 GeV) or by e.g. H.E.S.S., MAGIC and VERITAS in the very-high-energy band (VHE, 0.1 – 30 TeV) are mostly AGN belonging to the class of blazars. The non-thermal relativistic jets emitted by blazars are pointed along the line-of-sight, resulting in an enhancement of the gamma-ray flux and energy as observed on Earth. Subclasses of blazars include flat-spectrum radio quasars (FSRQs), low-frequency-peaked BL Lac objects (LBLs), intermediate-frequency-peaked BL Lac objects (IBLs), and high-frequency-peaked BL Lac objects (HBLs). The energy of the peak gamma-ray

¹ jbiteau@ucsc.edu

² daw@ucsc.edu

emission increases from FSRQs to HBLs and the UV-O-IR photon fields encountered by gamma rays in the jets appears to be more and more suppressed along this sequence (Ghisellini et al. 1998), making BL Lacs ideal cosmological probes of the EBL (the case of FSRQs remains debated, see e.g. Reimer 2007).

The main difficulty in constraining the EBL from gamma-ray observations lies in the uncertainties on the spectrum emitted at the source as would be observed on Earth without absorption, the intrinsic spectrum. If some curvature is present in the observed spectrum, one could wonder whether it is related to the emission processes occurring in the blazar's jet or to absorption by the EBL during the propagation of the gamma rays to the Earth. Upper-limits on the EBL have been obtained assuming no intrinsic curvature, either in the VHE or HE-VHE spectra of the sources, as e.g. in Meyer et al. (2012) or Georganopoulos et al. (2010), and constraints have been placed with similar hypotheses by Orr et al. (2011) and Sinha et al. (2014). The intrinsic HE-VHE curvature is accounted for on a statistical basis in Sanchez et al. (2013), through a broad-band modeling of the source emission from X rays to VHE in Domínguez et al. (2013) following a method suggested by Mankuzhiyil et al. (2010), by extrapolating the unabsorbed part of the HE spectrum in Ackermann et al. (*Fermi*-LAT Collaboration, 2012), and by leaving the VHE curvature as a free parameter in H.E.S.S. Collaboration (2013f). In particular, the *Fermi*-LAT and H.E.S.S. collaborations detected the imprint of the absorption by the EBL at the 6 standard deviation (σ) level and at the 9σ level, respectively. Their approach is based on the scaling of existing EBL models via a normalization factor that, if significantly different from zero, indicates the best level of absorption by the EBL compatible with the gamma-ray data. The present work aims to overcome this model-dependent approach and to provide a broad-band EBL spectrum.

We first show in Sec. 2 that the optical depth calculated from the EBL spectrum can largely be simplified. One of the three integrals in the relation is fully reducible in an analytical way. We further show that the EBL spectrum can be deconvoluted from the pair-creation smearing effect, under the assumption of a simplified evolution of the EBL (which we validate in Appendix A). Section 3 presents the dataset studied. The results are discussed in Sec. 4, with Sec. 4.1 focusing on the EBL spectrum and the room left for reionization sources or truly diffuse components. We propose a model-independent method to constrain the Hubble constant in Sec. 4.2. We investigate the redshifts of under-constrained sources in Sec. 4.3. And finally, we search for anomalies that could originate from axion-like particles and from Lorentz invariance violation in Sec. 4.4 and 4.5. More details on the systematic uncertainties, best-fit parameters, and gamma-ray residuals are provided in appendices.

2. EBL OPTICAL DEPTH

The EBL optical depth to gamma rays of energy E_0 (in the lab frame) emitted by a source at redshift z_0 is

given by:

$$\tau(E_0, z_0) = \int_0^{z_0} dz \frac{\partial L}{\partial z}(z) \int_0^\infty d\epsilon \frac{\partial n}{\partial \epsilon}(\epsilon, z) \int_{-1}^1 d\mu \frac{1-\mu}{2} \sigma_{\gamma\gamma}[\beta(E_0, z, \epsilon, \mu)] \quad (1)$$

where $\partial n/\partial \epsilon$ is the density of EBL photons per infinitesimal energy band at energy ϵ and redshift z . The other terms are defined in the following.

Assuming a flat Λ CDM cosmology, with Hubble constant H_0 , matter density Ω_M and dark energy density Ω_Λ , the distance element is:

$$\frac{\partial L}{\partial z} = \frac{c}{H_0} \frac{1}{1+z} \frac{1}{\sqrt{\Omega_\Lambda + \Omega_M(1+z)^3}} \equiv \frac{c}{H_0} \frac{\partial l}{\partial z} \quad (2)$$

The integration over the energy of the EBL photons in Eq. 1 is performed above the pair-creation threshold energy (see e.g. Eq. 8 in Gould & Schröder 1967a) and this information is encoded in the Bethe-Heitler cross section, with $\beta \in [0, 1]$:

$$\sigma_{\gamma\gamma}(\beta) = \frac{3\sigma_T}{16} (1-\beta^2) \left[-4\beta + 2\beta^3 + (3-\beta^4) \ln \frac{1+\beta}{1-\beta} \right] \quad (3)$$

with σ_T the Thomson cross section and where

$$\beta^2 = 1 - \frac{2m_e^2 c^4}{E_0 \epsilon} \frac{1}{1+z} \frac{1}{1-\mu} \quad (4)$$

with m_e mass of the electron and where μ is the cosine of the angle between the gamma ray and the EBL photons.

Calling $\epsilon_0 = \epsilon/(1+z)$ the energy of the EBL photons as measured today, $\beta^2 \geq 0$ is equivalent to:

$$(1+z)^2 \frac{E_0 \epsilon_0}{m_e^2 c^4} \geq 1 \quad (5)$$

which is the pair-creation threshold condition.

The definition of the EBL optical depth in Eq. 1 requires an integration over the distance, the energy of the EBL photons, and the angle between the EBL photons and the gamma ray. We show here that one integration can be reduced in a fully analytical way without any loss of generality. Using the change of variables¹ $\mu \rightarrow \beta$, the optical depth indeed reads:

$$\tau(E_0, z_0) = \frac{3}{4} \frac{\sigma_T c}{H_0} \int_0^{z_0} dz \frac{\partial l}{\partial z}(z) \int_0^\infty d\epsilon \frac{\partial n}{\partial \epsilon}(\epsilon, z) \frac{1}{(1+z)^2} \left(\frac{m_e^2 c^4}{E_0 \epsilon} \right)^2 P(\beta_{\max}) \quad (6)$$

with $\beta_{\max}^2 = 1 - \frac{m_e^2 c^4}{E_0 \epsilon} \frac{1}{1+z}$, and where the particle-physics kernel P admits, after integration over β , the

¹ This differs from the change of variable of Nikishov (1962) and Gould & Schröder (1967a) who use $\mu \rightarrow s = (1-\beta^2)^{-1}$.

following analytical expression:

$$\begin{aligned}
 P(x) = & \ln^2 2 - \frac{\pi^2}{6} + 2 \operatorname{Li}_2\left(\frac{1-x}{2}\right) - \frac{x+x^3}{1-x^2} \\
 & + (\ln(1+x) - 2\ln 2) \ln(1-x) \\
 & + \frac{1}{2} (\ln^2(1-x) - \ln^2(1+x)) \\
 & + \frac{1+x^4}{2(1-x^2)} \ln \frac{1+x}{1-x}
 \end{aligned} \quad (7)$$

where $\operatorname{Li}_2(x)$ is the dilogarithm.

This important result already eases the computation of the optical depth for a given cosmology and EBL evolution. Going further requires an approximation: as in Madau & Phinney (1996), we assume that the evolution and spectrum of the EBL can be locally decoupled, i.e.

$$d\epsilon \frac{\partial n}{\partial \epsilon}(\epsilon, z) = d\epsilon_0 \frac{\partial n}{\partial \epsilon_0}(\epsilon_0, 0) \times \text{evol}(z) \quad (8)$$

where $\text{evol}(z)$ parametrizes the EBL history. We show in Appendix A.1 that this approximation mildly impacts the optical depth up to redshifts² of $z \sim 0.6$.

Changing the variable $\epsilon_0 \rightarrow e_0 = \ln(E_0 \epsilon_0 / m_e^2 c^4)$, the EBL optical depth can be written as the convolution product:

$$\begin{aligned}
 \tau(E_0, z_0) &= \frac{3\pi\sigma_T}{H_0} \times \frac{E_0}{m_e^2 c^4} \times \\
 &\int_{-\infty}^{\infty} de_0 \nu I_\nu \left(e_0 - \ln \frac{E_0}{m_e c^2} \right) \times K_{z_0}(e_0) \\
 &= \frac{3\pi\sigma_T}{H_0} \times \frac{E_0}{m_e^2 c^4} \times \nu I_\nu \otimes K_{z_0} \left(\ln \frac{E_0}{m_e c^2} \right)
 \end{aligned} \quad (9)$$

where $\nu I_\nu = c/4\pi \times \epsilon_0^2 \partial n / \partial \epsilon_0$ is the EBL specific intensity at $z = 0$ as a function of $\ln(\epsilon_0 / m_e c^2) = \ln(h\nu / m_e c^2)$, and where the EBL kernel is:

$$\begin{aligned}
 K_{z_0}(e_0) &= \exp(-3e_0) \int_0^{z_0} dz \frac{\partial l}{\partial z}(z) \times \frac{\text{evol}(z)}{(1+z)^4} \\
 &\times P \left(\sqrt{1 - \frac{\exp(-e_0)}{(1+z)^2}} \right)
 \end{aligned} \quad (10)$$

Following Raue & Mazin (2008), we parametrize the evolution of the EBL as $\text{evol}(z) = (1+z)^{3-f_{\text{evol}}}$, where f_{evol} quantifies the impact of the sources. For example, $f_{\text{evol}} = 0$ would correspond to a simple cosmological expansion of the photon field with no source term. Assuming a flat Λ CDM cosmology with $\Omega_\Lambda = 0.7$, $\Omega_M = 0.3$, $H_0 = 70 \text{ km s}^{-1} \text{ Mpc}^{-1}$, we show in Appendix A.1 that $f_{\text{evol}} = 1.7$ best reproduces the evolutions of the EBL models of Franceschini et al. (2008) and Gilmore et al. (2012). These two state-of-the-art models from independent groups have been chosen to calibrate our approach, and we note that using a different model (e.g. Domínguez et al. 2011b, closer to $f_{\text{evol}} = 1.2$) has a minimal impact on our results, well below the uncertainties quoted in the following.

² This parametrization remains acceptable up to $z \sim 0.8$ for optical depths smaller than 2–3.

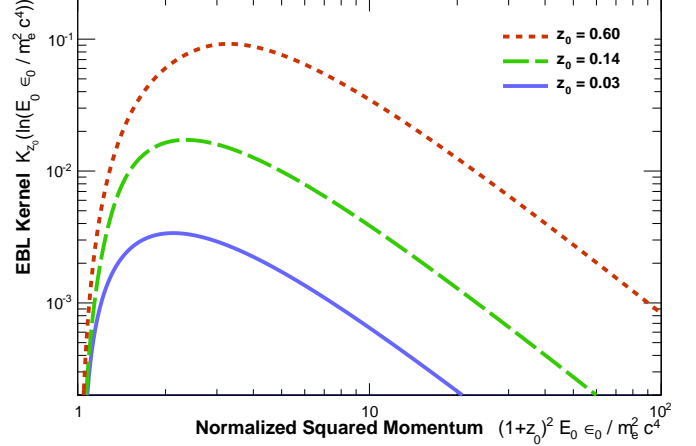


FIG. 1.— EBL kernel, which yields the gamma-ray optical depth after convolution with the EBL intensity, as a function of the product of gamma-ray and EBL-photon energies in electron-mass units, in the lab frame.

The EBL kernel from Eq. 10 is shown in Fig. 1 as a function of the squared momentum of the interacting photons (EBL and gamma ray), normalized to twice the squared electron mass. Below one, the pair creation threshold condition in Eq. 5 is not satisfied, resulting in a null kernel. The kernel peaks between 2 and 4 times the threshold with a peak position and amplitude increasing with redshift. Note that for a fixed gamma-ray energy, the full width at half maximum of the EBL kernel almost spans an order of magnitude in EBL-photon energy (or equivalently in wavelength), whatever the redshift. This broadness argues against simple delta-function approximations to reconstruct the EBL spectrum, such as assumed in Sinha et al. (2014). This also implies that any spectral reconstruction of the EBL based on gamma-ray observations yields correlated flux estimates across the probed wavelength range, though these correlations can be fully taken into account in further analyses, as demonstrated e.g. in Sec. 4.2.

Having shown that the EBL optical depth can be written as the convolution product in Eq. 9, we measure in the following the broad-band EBL spectrum based on local constraints and on gamma-ray absorption observed in gamma-ray spectra of blazars.

3. DATASET AND ANALYSIS

3.1. Local constraints

Direct constraints on the intensity of the EBL from UV-O-IR observations come in two flavors: lower limits derived from galaxy counts, where faint emitters or truly diffuse components can be missed; and upper limits derived from direct measurements, which are contaminated by bright foregrounds (zodiacal and Galactic light), at least below $100 \mu\text{m}$. In the following, we exploit the extensive bibliographic study of Dwek & Krennrich (2013). We select state-of-the-art constraints from independent datasets, resulting in 27 upper limits and 25 lower limits (called local constraints in the following). For the latter, we select the estimates corrected for the completeness of the sample. These data are reproduced in Table 1, with uncertainties combining statistical and systematic

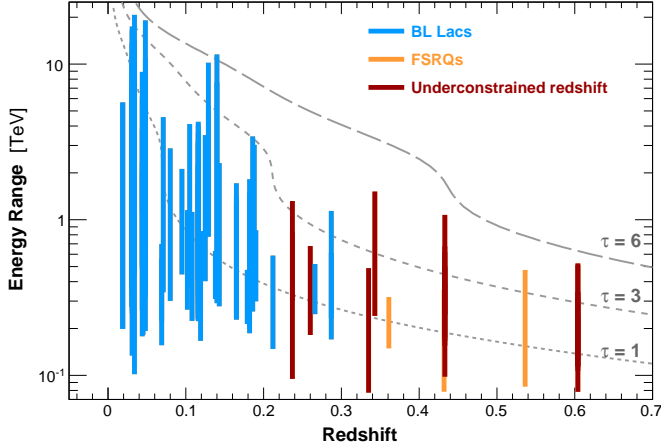


FIG. 2.— Energy ranges spanned by the spectra from Table 2 as a function of redshift.

uncertainties. In addition to constraints listed by Dwek & Krennrich (2013), we also include the lower limits at $3.6 \mu\text{m}$ and $4.5 \mu\text{m}$ from Ashby et al. (2013).

3.2. Gamma-ray data

We study the gamma-ray spectra of blazars published by ground based instruments up to 2014. We have succeeded in obtaining the spectral points for 106 non-redundant spectra, listed in Table 2, from 38 sources. Representing more than 80 % of the spectral data from blazars indexed in TeVCat,³ this is the most complete compilation of VHE gamma-ray data ever used for a study of the EBL. We paid particular attention to redundant data published in multiple articles, and selected the most up-to-date ones when a reanalysis was performed or when new data were included in the study.

To perform cosmological studies, we therefore select the spectra of known-redshift BL Lac objects, called the gamma-ray cosmology sample in the following. With a total of $\sim 270,000$ gamma rays from 86 spectra, this sample carries most of the information on gamma-ray absorption. The remaining 20 spectra, contributing an additional $\sim 30,000$ gamma rays, are used in Sections 4.3 and 4.4.

The energy ranges spanned by the gamma-ray spectra are shown in Fig. 2, together with the iso-optical-depth lines derived from our best-fit EBL spectrum (see Sec. 4.1). The full sample covers a redshift range up to $z \sim 0.604$ (PKS 1424+240) while the gamma-ray cosmology sample is limited to $z \leq 0.287$ (1ES 0414+009).

Six objects have uncertain redshifts, shown as red lines in Fig. 2 and indicated by a question mark in the third column of Table 2. They are discussed in more detail in Sec. 4.3.

We also associated a quasi-contemporaneous HE gamma-ray spectrum to each VHE spectrum whenever available. In particular, VHE observations performed after mid-2008 are contemporaneous with the sky survey of *Fermi*-LAT. Whenever HE best-fit spectral parameters were published in the same article as the VHE spectrum, we stored them for further analysis. The same

procedure was followed using the 2FGL spectra (Nolan et al. 2012) for objects showing no significant variability in both gamma-ray bands, as long as the ground-based observations succeeded the launch of the satellite.

The quasi-contemporaneity of HE and VHE data motivates the use of the HE spectral shape to constrain the intrinsic VHE model. Photon indices have proven quite stable in the HE band except during flaring events, despite the rather high flux variability at all time scales that is characteristic of blazars (see, e.g., Abdo et al. 2010).

3.3. Analysis method

3.3.1. Test statistic

We aim at finding the best EBL spectrum jointly accounting for local constraints and gamma-ray observations. We define the associated test statistic as:

$$\chi^2 = \chi_{\text{EBL}}^2 + \sum_{\gamma\text{-ray spectra}} (\chi_{\gamma\text{-ray points}}^2 + \chi_{\text{HE-VHE}}^2) \quad (11)$$

$\chi_{\gamma\text{-ray points}}^2$ is a measure of the quality of the fit of each gamma-ray spectrum:

$$\chi_{\gamma\text{-ray points}}^2 = \sum_{i \in \gamma\text{-ray points}} \left(\frac{\phi_{\text{model}}(E_i, z_0) - \phi_i}{\sigma_{\phi_i}} \right)^2 \quad (12)$$

where ϕ_i and σ_{ϕ_i} are the measured flux and associated uncertainty, and where ϕ_{model} is discussed in Sec. 3.3.2.

$\chi_{\text{HE-VHE}}^2$ accounts for the constraints on the intrinsic spectral parameters. We impose, for contemporaneous observations in the HE and VHE bands, that the intrinsic VHE spectrum be softer than the HE spectrum:

$$\chi_{\text{HE-VHE}}^2 = \Theta(\Gamma_{\text{HE}} - \Gamma) \left(\frac{\Gamma_{\text{HE}} - \Gamma}{\sigma_{\Gamma_{\text{HE}}}} \right)^2 \quad (13)$$

where Γ_{HE} and $\sigma_{\Gamma_{\text{HE}}}$ are the photon index and associated uncertainty measured at HE, and where Γ is the intrinsic VHE photon index. For curved spectra, the indices and uncertainties are computed at the intersection of the HE and VHE range.

χ_{EBL}^2 accounts for the lower limits and upper limits listed in Table 1, $\left\{ \nu I_{\nu}^i \pm \sigma_{\nu I_{\nu}}^i \right\}_i$. Only the constraining sides of the limits are considered, using again Heavyside functions:

$$\begin{aligned} \chi_{\text{EBL}}^2 = & \sum_{i \in \text{LL}} \Theta(\nu I_{\nu}^i - \nu I_{\nu}(\lambda_i)) \times \left(\frac{\nu I_{\nu}(\lambda_i) - \nu I_{\nu}^i}{\sigma_{\nu I_{\nu}}^i} \right)^2 \\ & + \sum_{i \in \text{UL}} \Theta(\nu I_{\nu}(\lambda_i) - \nu I_{\nu}^i) \times \left(\frac{\nu I_{\nu}(\lambda_i) - \nu I_{\nu}^i}{\sigma_{\nu I_{\nu}}^i} \right)^2 \end{aligned} \quad (14)$$

where $\nu I_{\nu}(\lambda)$ is the model of the data, and where LL and UL denote the ensembles of lower and upper limits, respectively.

The local constraints effectively taken into account in Eq. 14 depend on the EBL-wavelength range probed by the gamma-ray data. The threshold condition in Eq. 5 imposes $\lambda = hc/\epsilon_0 < \lambda_{\text{max}}$, where λ_{max} is the maximum

³ <http://tevcat.uchicago.edu/>

TABLE 1
LOCAL CONSTRAINTS ON THE EBL SPECTRUM USED IN THIS PAPER, LARGELY EXTRACTED FROM DWEK & KRENNRICH (2013).

λ μm	Lower limit $\text{nW m}^{-2} \text{sr}^{-1}$	Upper limit $\text{nW m}^{-2} \text{sr}^{-1}$	Experiment	Reference
0.153	1.03 ± 0.15	...	Galex	Xu et al. (2005)
0.1595	3.75 ± 1.25	...	HST/WFPC2	Gardner et al. (2000)
0.231	2.25 ± 0.32	...	Galex	Xu et al. (2005)
0.2365	3.6 ± 0.5	...	HST/WFPC2	Gardner et al. (2000)
0.3	...	18 ± 12	HST/WFPC2	Bernstein (2007)
0.3	3.7 ± 0.7	...	HST+ground	Totani et al. (2001)
0.4	...	26 ± 10	dark cloud	Mattila (1990)
0.44	...	7.9 ± 4.0	Pioneer 10/11	Matsuoka et al. (2011)
0.45	6.1 ± 1.8	...	HST+ground	Totani et al. (2001)
0.5115	...	30 ± 9	ground	Dube et al. (1979)
0.55	...	55 ± 27	HST/WFPC2	Bernstein (2007)
0.61	7.4 ± 1.5	...	HST+ground	Totani et al. (2001)
0.64	...	7.7 ± 5.8	Pioneer 10/11	Matsuoka et al. (2011)
0.81	9.3 ± 1.6	...	HST+ground	Totani et al. (2001)
0.814	...	57 ± 32	HST/WFPC2	Bernstein (2007)
1.25	...	21 ± 15	COBE/DIRBE	Levenson et al. (2007)
1.25	11.5 ± 1.3	...	HST+ground	Totani et al. (2001)
1.25	11.7 ± 2.6	...	Subaru	Keenan et al. (2010)
1.6	11.5 ± 1.5	...	Subaru	Keenan et al. (2010)
2.12	10.0 ± 0.8	...	Subaru	Keenan et al. (2010)
2.2	...	20 ± 6	COBE/DIRBE	Levenson et al. (2007)
2.2	9.0 ± 1.2	...	HST+ground	Totani et al. (2001)
3.5	...	13.3 ± 2.8	COBE/DIRBE	Levenson et al. (2007)
3.6	5.6 ± 1.0	...	Spitzer/IRAC	Ashby et al. (2013)
4.5	4.4 ± 0.8	...	Spitzer/IRAC	Ashby et al. (2013)
4.9	...	22 ± 12	COBE/DIRBE	Arendt & Dwek (2003)
15	1.9 ± 0.4	...	ISO/ISOCAM	Hopwood et al. (2010)
16	2.2 ± 0.2	...	Spitzer	Teplitz et al. (2011)
24	$2.86^{+0.19}_{-0.16}$...	Spitzer/MIPS	B��thermin et al. (2010)
60	...	28.1 ± 7.2	COBE/DIRBE	Finkbeiner et al. (2000)
65	...	12.5 ± 9.3	Akari	Matsuura et al. (2011)
70	$6.6^{+0.7}_{-0.6}$...	Spitzer/MIPS	B��thermin et al. (2010)
90	...	22.3 ± 5.0	Akari	Matsuura et al. (2011)
100	8.35 ± 0.95	...	Herschel/PACS	Berta et al. (2011)
140	...	12.6 ± 6.0	COBE/FIRAS	Fixsen et al. (1998)
140	...	20.1 ± 3.6	Akari	Matsuura et al. (2011)
140	...	15.0 ± 5.9	COBE/DIRBE	Odegard et al. (2007)
160	$14.6^{+7.1}_{-2.9}$...	Spitzer/MIPS	B��thermin et al. (2010)
160	...	13.7 ± 6.1	COBE/FIRAS	Fixsen et al. (1998)
160	...	13.7 ± 4.0	Akari	Matsuura et al. (2011)
160	...	14.4 ± 2.4	Spitzer/MIPS	P��nin et al. (2012)
240	...	10.9 ± 4.3	COBE/FIRAS	Fixsen et al. (1998)
240	...	12.7 ± 1.6	COBE/DIRBE	Odegard et al. (2007)
250	$10.13^{+2.60}_{-2.33}$...	Herschel/SPIRE	B��thermin et al. (2012)
250	...	10.3 ± 4.0	COBE/FIRAS	Fixsen et al. (1998)
350	$6.46^{+1.74}_{-1.57}$...	Herschel/SPIRE	B��thermin et al. (2012)
350	...	5.6 ± 2.1	COBE/FIRAS	Fixsen et al. (1998)
500	$2.80^{+0.93}_{-0.81}$...	Herschel/SPIRE	B��thermin et al. (2012)
500	...	2.4 ± 0.9	COBE/FIRAS	Fixsen et al. (1998)
850	0.24 ± 0.03	...	SCUBA	Zemcov et al. (2010)
850	...	0.50 ± 0.21	COBE/FIRAS	Fixsen et al. (1998)

wavelength associated with each spectrum, with:

$$\lambda_{\text{max}} = \frac{h}{m_e c} \times \frac{E_{\text{max,VHE}}}{m_e c^2} \times (1 + z_0)^2 \quad (15)$$

$$\sim 95 \mu\text{m} \times \left(\frac{E_{\text{max,VHE}}}{20 \text{ TeV}} \right) \times (1 + z_0)^2$$

The minimum wavelength is set *a posteriori* by successively adding free parameters to the model until no further improvement is found, as discussed in Sec. 3.3.3.

Expanding on the method of H.E.S.S. Collaboration (2013f), the minimization of the χ^2 in Eq. 11 in turn assumes, for each set of EBL parameters tested, a min-

imization over the parameters of the intrinsic spectra. This minimization is performed for each spectrum using the MIGRAD method of MINUIT. The minimization over the EBL parameters is performed in three steps, using successively SIMPLEX, MIGRAD, and HESSIAN.

3.3.2. Intrinsic spectral models

The VHE gamma-ray spectra are modeled with

$$\phi_{\text{model}}(E, z) = \phi_{\text{int}}(E) \times \exp(-\tau(E, z)) \quad (16)$$

The intrinsic model, $\phi_{\text{int}}(E)$, is determined iteratively as done by the H.E.S.S. Collaboration (2013f). As a first step, the simplest two-parameter model is cho-

sen: a power law (PWL in Table 2), $\phi_{\text{PWL}}(E) = \phi_0(E/E_0)^{-\Gamma}$, where E_0 is the reference energy, ϕ_0 is the flux normalization and Γ is the photon index. The reference energy is fixed, in this work, to the central value of the energy range of each spectrum, i.e. $E_0 = \sqrt{E_{\text{min,VHE}} E_{\text{max,VHE}}}$. To search for intrinsic curvature, we also test the three-parameter log parabola (LP), $\phi_{\text{LP}}(E) = \phi_0(E/E_0)^{-a-b \ln(E/E_0)}$, where a is the photon index at E_0 and where b is the curvature parameter, the exponential cutoff power law (EPWL), $\phi_{\text{EPWL}}(E) = \phi_0(E/E_0)^{-\Gamma} \exp(-E/E_{\text{cut}})$, where E_{cut} is the cutoff energy. We also consider an exponential cutoff log parabola (ELP), $\phi_{\text{ELP}}(E) = \phi_0(E/E_0)^{-a-b \ln(E/E_0)} \exp(-E/E_{\text{cut}})$, however none of

the spectra is found to significantly prefer this model. We impose concave intrinsic spectra, i.e. $b \geq 0$ and $E_{\text{cut}} > 0$.

For a given set of intrinsic models, we inspect the residuals of the individual spectra fixing the EBL parameters to their best-fit values. If a more complex intrinsic model is preferred at least at the 2σ level, it is chosen for the next iteration, until the set of models converges. To avoid any overrestriction of the parameter space, once the stable set of intrinsic models was found, we successively changed each intrinsic spectrum to its more complex counterpart, whichever was most preferred, and checked that it had no impact on other models nor on the best-fit EBL spectrum. This ensured the robustness of our method and of the choice of the intrinsic models.

TABLE 2
GAMMA-RAY SPECTRA USED IN THIS PAPER.

Source	Class	Redshift	Experiment	Obs. Period	Model	Reference
IC 310	HBL	0.019	MAGIC	2009-2010 (low)	PWL	Aleksić et al. (2014b)
...	MAGIC	2009-2010 (high)	PWL	Aleksić et al. (2014b)
Markarian 421	HBL	0.031	CAT	1998	PWL	Piron & CAT Collab. (2000)
...	HEGRA	1999-2000	PWL	Aharonian et al. (2002)
...	HEGRA	2000-2001	LP	Aharonian et al. (2002)
...	Tibet	2000-2001	PWL	Amenomori et al. (2003)
...	HESS	2004	EPWL	Aharonian et al. (2005c)
...	MAGIC	2004-2005	EPWL	Albert et al. (2007d)
...	MAGIC	2006-04-22	PWL	Aleksić et al. (2010)
...	MAGIC	2006-04-24	PWL	Aleksić et al. (2010)
...	MAGIC	2006-04-25	PWL	Aleksić et al. (2010)
...	MAGIC	2006-04-26	PWL	Aleksić et al. (2010)
...	MAGIC	2006-04-27	EPWL	Aleksić et al. (2010)
...	MAGIC	2006-04-28	PWL	Aleksić et al. (2010)
...	MAGIC	2006-04-29	PWL	Aleksić et al. (2010)
...	ARGO-YBJ	2007-2010 (flux1)	PWL	Bartoli et al. (2011)
...	ARGO-YBJ	2007-2010 (flux2)	LP	Bartoli et al. (2011)
...	ARGO-YBJ	2007-2010 (flux3)	EPWL	Bartoli et al. (2011)
...	ARGO-YBJ	2007-2010 (flux4)	PWL	Bartoli et al. (2011)
...	VERITAS	2008 (very low)	LP	Acciari et al. (2011b)
...	VERITAS	2008 (low)	LP	Acciari et al. (2011b)
...	VERITAS	2008 (mid)	LP	Acciari et al. (2011b)
...	VERITAS	2008 (high A)	LP	Acciari et al. (2011b)
...	VERITAS	2008 (high B)	EPWL	Acciari et al. (2011b)
...	VERITAS	2008 (high C)	PWL	Acciari et al. (2011b)
...	VERITAS	2008 (very high)	EPWL	Acciari et al. (2011b)
...	TACTIC	2005-2006	PWL	Sharma et al. (2015)
...	TACTIC	2008	PWL	Chandra et al. (2010)
...	TACTIC	2009-2010	PWL	Chandra et al. (2012)
Markarian 501	HBL	0.034	HEGRA	1997	PWL	Aharonian et al. (2001)
...	TACTIC	2005-2006	PWL	Godambe et al. (2008)
...	MAGIC	2006	PWL	Anderhub et al. (2009b)
...	ARGO-YBJ	2008-2011	PWL	Bartoli et al. (2012)
...	ARGO-YBJ	2011 (high)	PWL	Bartoli et al. (2012)
1ES 2344+514	HBL	0.044	Whipple	1995 (dataset B)	PWL	Schroedter et al. (2005)
...	MAGIC	2005-2006	PWL	Albert et al. (2007c)
...	VERITAS	2007 (low)	LP	Acciari et al. (2011a)
...	VERITAS	2007 (high)	PWL	Acciari et al. (2011a)
...	MAGIC	2008	PWL	Aleksić et al. (2013)
Markarian 180	HBL	0.045	MAGIC	2006	PWL	Albert et al. (2006)
1ES 1959+650	HBL	0.048	HEGRA	2002	PWL	Aharonian et al. (2003a)
...	Whipple	2002	PWL	Daniel et al. (2005)
...	MAGIC	2006	PWL	Tagliaferri et al. (2008)
...	VERITAS	2007-2011	PWL	Aliu et al. (2013b)
BL Lacertae	IBL	0.069	MAGIC	2005	PWL	Albert et al. (2007a)
...	VERITAS	2011	PWL	Arlen et al. (2013)
PKS 2005-489	HBL	0.071	HESS	2004-2007	PWL	H.E.S.S. Collaboration (2010b)
RGB J0152+017	HBL	0.08	HESS	2007	PWL	Aharonian et al. (2008a)
SHBL J001355.9-185406	HBL	0.095	HESS	2008-2011	PWL	H.E.S.S. Collaboration (2013a)
W Comae	IBL	0.102	VERITAS	2008-01-04	PWL	Acciari et al. (2008)
1ES 1312-423	HBL	0.105	HESS	2004-2010	PWL	H.E.S.S. Collaboration (2013d)
VER J0521+211	IBL	0.108	VERITAS	2009-2010	PWL	Archambault et al. (2013)
PKS 2155-304	HBL	0.116	HESS	2002-06	PWL	Aharonian et al. (2005a)
...	HESS	2002-10	PWL	Aharonian et al. (2005a)
...	HESS	2003-06	PWL	Aharonian et al. (2005a)

TABLE 2 — *Continued*

Source	Class	Redshift	Experiment	Obs. Period	Model	Reference
...	HESS	2003-07	PWL	Aharonian et al. (2005a)
...	HESS	2003-08	PWL	Aharonian et al. (2005a)
...	HESS	2003-09	PWL	Aharonian et al. (2005a)
...	HESS	2003-10-11	PWL	Aharonian et al. (2005b)
...	HESS	2005-2007	PWL	H.E.S.S. Collaboration (2010c)
...	HESS	2006-07/08	LP	Abramowski et al. (2013)
...	MAGIC	2006-07/08	LP	Aleksić et al. (2012c)
...	HESS	2006-08-02	PWL	H.E.S.S. Collaboration (2012a)
...	HESS	2006-08-03	PWL	H.E.S.S. Collaboration (2012a)
...	HESS	2008-08-09	PWL	Aharonian et al. (2009)
B3 2247+381	HBL	0.119	MAGIC	2010	PWL	Aleksić et al. (2012a)
RGB J0710+591	HBL	0.125	VERITAS	2008-2009	PWL	Acciari et al. (2010b)
H 1426+428	HBL	0.129	HEGRA	1999-2000	PWL	Aharonian et al. (2003b)
...	HEGRA	2002	PWL	Aharonian et al. (2003b)
1ES 0806+524	HBL	0.138	VERITAS	2006-2008	PWL	Acciari et al. (2009a)
1ES 0229+200	HBL	0.14	HESS	2005-2006	PWL	Aharonian et al. (2007c)
...	VERITAS	2009-2012	PWL	Aliu et al. (2014)
1RXS J101015.9-311909	HBL	0.143	HESS	2006-2010	PWL	H.E.S.S. Collaboration (2012c)
H 2356-309	HBL	0.165	HESS	2004	PWL	H.E.S.S. Collaboration (2010a)
...	HESS	2005	PWL	H.E.S.S. Collaboration (2010a)
...	HESS	2006	PWL	H.E.S.S. Collaboration (2010a)
RX J0648.7+1516	HBL	0.179	VERITAS	2010	PWL	Aliu et al. (2011)
1ES 1218+304	HBL	0.182	VERITAS	2007	PWL	Acciari et al. (2009b)
...	VERITAS	2008-2009	PWL	Acciari et al. (2010a)
1ES 1101-232	HBL	0.186	HESS	2004-2005	PWL	Aharonian et al. (2007a)
1ES 0347-121	HBL	0.188	HESS	2006-09-12	PWL	Aharonian et al. (2007b)
RBS 0413	HBL	0.19	VERITAS	2008-2009	PWL	Aliu et al. (2012a)
1ES 1011+496	HBL	0.212	MAGIC	2007	PWL	Albert et al. (2007b)
1ES 1215+303	HBL	0.237?	VERITAS	2008-2012	PWL	Aliu et al. (2013a)
...	MAGIC	2011	PWL	Aleksić et al. (2012b)
S5 0716+714	IBL	0.26?	MAGIC	2007-2008	PWL	Anderhub et al. (2009a)
PKS 0301-243	HBL	0.266	HESS	2009-2010	PWL	H.E.S.S. Collaboration (2013c)
1ES 0414+009	HBL	0.287	HESS	2005-2009	PWL	H.E.S.S. Collaboration (2012b)
...	VERITAS	2008-2011	PWL	Aliu et al. (2012b)
3C 66A	IBL	0.335?	MAGIC	2009-2010	PWL	Aleksić et al. (2011b)
PKS 0447-439	HBL	0.343?	HESS	2009-2010	PWL	H.E.S.S. Collaboration (2013b)
PKS 1510-089	FSRQ	0.361	HESS	2009	PWL	H.E.S.S. Collaboration (2013e)
4C +21.35	FSRQ	0.432	MAGIC	2010-06-17	PWL	Aleksić et al. (2011a)
PG 1553+113	HBL	0.433?	HESS	2005-2006	PWL	Aharonian et al. (2008b)
...	MAGIC	2007	PWL	Aleksić et al. (2012d)
...	MAGIC	2008	PWL	Aleksić et al. (2012d)
...	MAGIC	2009	PWL	Aleksić et al. (2012d)
...	VERITAS	2010-2012	PWL	Aliu et al. (2015)
...	HESS	2012	PWL	Abramowski et al. (2015)
3C 279	FSRQ	0.536	MAGIC	2006	PWL	MAGIC Collaboration (2008)
PKS 1424+240	IBL	0.604?	VERITAS	2009	PWL	Archambault et al. (2014)
...	VERITAS	2011	PWL	Archambault et al. (2014)
...	VERITAS	2013	PWL	Archambault et al. (2014)
...	MAGIC	2009	PWL	Aleksić et al. (2014a)
...	MAGIC	2010	PWL	Aleksić et al. (2014a)
...	MAGIC	2011	PWL	Aleksić et al. (2014a)

$$\begin{aligned}
\nu I_\nu(l) &= \sum_i a_i \exp\left(-\frac{(l-l_i)^2}{2\sigma_l^2}\right) \\
&\equiv \sum_i a_i \mathcal{N}(l; l_i, \sigma_l)
\end{aligned} \tag{17}$$

3.3.3. Deconvolution method

Similarly to the splines used in Mazin & Raue (2007), we chose a spectral model for the EBL that is a linear function of its parameters. As shown in Eq. 9, the pertinent variable is the logarithm of the EBL-photon energy, or equivalently the logarithm of the EBL wavelength $l = \ln(\lambda/\lambda_{\text{ref}})$, where λ_{ref} is a reference wavelength, set e.g. to $1\mu\text{m}$. We model the EBL intensity as a sum of Gaussians of this variable, with fixed widths and peak positions:

The peak positions are logarithmically spaced:

$$\log(\lambda_i/\lambda_{\text{ref}}) \equiv l_i = l_0 + i \times \Delta_l \tag{18}$$

The width of the Gaussian functions depends on the distance between anchor points Δ_l . We impose that the sum of two consecutive Gaussians of unity amplitude be equal to one right in between the two anchor points, i.e.

$$\Delta_l = \sigma_l \times 2\sqrt{2\ln 2} \tag{19}$$

The Gaussians leak into the neighboring bins and the

average flux νI_ν^i in a bin centered on l_i is then

$$\begin{aligned} \nu I_\nu^i &= \sum_j a_j \frac{1}{\Delta_l} \int_{l_i - \Delta_l/2}^{l_i + \Delta_l/2} dl \exp\left(-\frac{(l - l_j)^2}{2\sigma_l^2}\right) \\ &\equiv \sum_j a_j w_{ij} \end{aligned} \quad (20)$$

with

$$\begin{aligned} w_{ij} &= \frac{\sqrt{\pi}}{4\sqrt{\ln 2}} \left[\operatorname{erf}\left(\left(i - j + \frac{1}{2}\right) \times 2\sqrt{\ln 2}\right) \right. \\ &\quad \left. - \operatorname{erf}\left(\left(i - j - \frac{1}{2}\right) \times 2\sqrt{\ln 2}\right) \right] \end{aligned} \quad (21)$$

The parameters a_i are left free to vary. Once best-fit values, uncertainties, and correlations have been determined, the binned average flux νI_ν^i can easily be derived from the linear relation in Eq. 20. This linearity permits the propagation of uncertainties for Gaussian distributions of the weight a_i , fully accounting for the correlation terms. This justifies the use of the HESSIAN method in Sec. 3.3.1, which yields such symmetric Gaussian uncertainties.

Given the linearity of the model with respect to its parameters a_i , the optical depth can be rewritten as:

$$\tau(E_0, z_0) = \sum_i a_i t_i(E_0, z_0) \quad (22)$$

where

$$\begin{aligned} t_i(E_0, z_0) &= \frac{3\pi\sigma_T}{H_0} \times \frac{E_0}{m_e c^4} \\ &\times \mathcal{N}(\cdot; 0, \sigma_l) \otimes K_{z_0} \left(e_i + \ln \frac{E_0}{m_e c^2} \right) \end{aligned} \quad (23)$$

where $e_i = \ln \frac{hc/\lambda_i}{m_e c^2}$.

One can compute the weights $t_i(E_0, z_0)$ in the very beginning of the fitting procedure, further reducing the computation expense. For a set of about 90 spectra and associated models, the full fitting procedure of the EBL spectrum takes about ten seconds of CPU time on a 3 GHz core, highlighting the significance of the analytical work shown in this section and in Sec. 2.

4. RESULTS

4.1. EBL spectrum

The best-fit spectral models of the intrinsic spectra are listed in column 6 of Table 2. Most of the spectra of the gamma-ray cosmology sample (71/86) are best described by PWL models. The other fifteen spectra, modeled by LP and EPWL models, correspond either to intensive campaigns in low states of prominent sources (2004-05 MAGIC campaign of Markarian 421, large-zenith-angle H.E.S.S. observations of Markarian 421, 2007 VERITAS campaign on 1ES 2344+514, 2007-2010 campaign of ARGO-YBG on Markarian 421: Albert et al. 2007d; Aharonian et al. 2005c; Acciari et al. 2011a; Bartoli et al. 2011, respectively), to observations of flares (high state of Markarian 421 observed by HEGRA in 2000-2001 and MAGIC in 2004-2005, major outburst of PKS 2155-304 in 2006 observed by MAGIC and H.E.S.S.: Aharonian

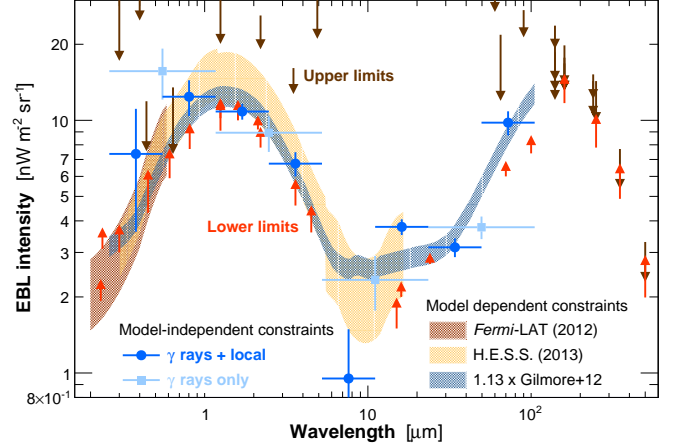


FIG. 3.— EBL intensity at $z = 0$ as a function of wavelength. The best-fit spectra derived in this work are shown with light blue (gamma rays only, four-point spectrum) and blue points (gamma rays + direct constraints, eight-point spectrum). Lower and upper limits are shown with orange upward-going and dark-brown downward-going arrows, respectively. For comparison with the work of Ackermann et al. (2012) and H.E.S.S. Collaboration (2013f), the 1σ (stat + sys) contour of the best-fit scaled-up model (Gilmore et al. 2012) is shown as filled blue region, using a scaling factor of 1.13 as shown in Table 4.

et al. 2002; Aleksić et al. 2010, 2012c; Abramowski et al. 2013, respectively), or to both (2006-2008 campaign on Markarian 421 by VERITAS, including flares: Abdo et al. 2011). In such cases, enhanced statistics at the highest energies enable the probe of intrinsic curvature. No spectrum is preferentially modeled with an ELP model.

The 86 spectra probe the wavelength range $0.26 - 105 \mu\text{m}$, for a bin size $\Delta_l = 0.75$. The maximum wavelength corresponds to the pair-creation threshold, as described in Eq. 15. A smaller minimum wavelength would result in an unconstrained EBL intensity in the first bin. A smaller binning does not significantly improve the quality of the fit. With a total of 630 points and 187 free parameters for the intrinsic spectra, the best-fit model results in a test statistic of $(\sum \chi_{\gamma\text{ray points}}^2 + \chi_{\text{HE-VHE}}^2)/ndf = 340.1/443$. The small value of the reduced χ^2 is not surprising, as the correlations between gamma-ray spectral points are not accounted for when fitting such archival data (the gamma-ray community is only starting to publish covariance matrices for spectral points). The uncertainties are also assumed to be Gaussian (underlying assumption for the χ^2 test), while a full treatment at the event level would account for the Poisson statistics of the events from background and signal regions.

The constraint from the hardness of the HE spectra associated with the VHE observations, proves *a posteriori* to play a minor role, $\sum \chi_{\text{HE-VHE}}^2 < 0.1$, indicating that there is no tension with the assumption of broad-band concavity in the intrinsic spectra. No tension is found with the local EBL constraints either, with $\chi_{\text{EBL}}^2 = 2.4$ to which $n_{\text{EBL}} = 7$ local constraints contribute. Both the local EBL constraint and the hardness constraint thus barely impact the best-fit estimate of the EBL spectrum, but they nonetheless play a significant role when the spectrum departs from the best-fit point, thus im-

pacting the uncertainties on the EBL. For the binning and the wavelength range probed here, the Gaussian-sum model admits eight parameters, resulting in a total test statistic of $\chi^2/\text{ndf} = 342.5/442$. The number of degrees of freedom accounts for eight free parameters to model the EBL and seven local points constraining this model, in addition to the 443 degrees of freedom accounting for the gamma-ray spectra.

Using the same intrinsic models and a null absorption, the gamma-ray spectra best-fit test statistic is $\sum(\chi_{\gamma\text{ray points}}^2 + \chi_{\text{HE-VHE}}^2) = 489.1$. With eight additional free parameters, the Gaussian-sum model is preferred by the gamma-ray data at the $\sqrt{2} \operatorname{erfc}^{-1}[\mathcal{P}_8(\Delta\chi^2 = 489.1 - 340.1)] = 11\sigma$ level, where \mathcal{P}_8 is the χ^2 probability for eight degrees of freedom. This significance level may not readily be interpreted as the detection significance of the EBL signature, because the intrinsic models chosen for the likelihood ratio test are based on the best-fit EBL spectrum. Conservatively choosing instead the intrinsic models based on fits directly to the observed spectra assuming no EBL absorption results in eight intrinsic models being changed to a more complex or an equally complex model. The best-fit EBL model is then preferred at the 10.3σ level, with no significant impact on the best-fit parameters. The cumulative EBL effect therefore leaves a strong imprint in the gamma-ray spectra, at a high significance level in between the two values given above. The EBL intensities computed from the best-fit parameters, as in Eq. 20, are listed in Table 3 and shown in Fig. 3 (blue points). The overall systematic uncertainty on the EBL level is estimated in Appendix A to be on the order of $7 - 8\%$.

TABLE 3
BEST FIT EBL INTENSITIES.

λ μm	λ_{\min} μm	λ_{\max} μm	νI_ν $\text{nW m}^{-2} \text{sr}^{-1}$
0.38	0.26	0.55	7.4 ± 3.7
0.80	0.55	1.2	12.4 ± 1.9
1.7	1.2	2.5	10.8 ± 0.8
3.6	2.5	5.2	6.7 ± 0.7
7.6	5.2	11	0.95 ± 0.53
16	11	23	3.79 ± 0.26
34	23	50	3.14 ± 0.25
72	50	105	9.8 ± 1.1

Theoretical and empirical EBL intensities can similarly be compared to local constraints and gamma-ray data. Table 4 lists the test statistics obtained with a null EBL, the best-fit eight-point EBL spectrum, and the models of Gilmore et al. (2012) (G12), Franceschini et al. (2008) (F08), Domínguez et al. (2011b) (D11), Stecker et al. (2006) (S06) Khaire & Srianand (2015) (KS14), Finke et al. (2010) (F10), and Kneiske & Dole (2010) (KD10). All the EBL models are preferred at the $10 - 12\sigma$ level to a null EBL (column 7), as computed from the improvement in the quality of the fit of the gamma-ray data (column 4). The EBL models can also be compared to the best-fit eight-point spectrum with a likelihood ratio test, assuming that the models are nested. Such an approach is justified by a difference in optical depth between a model and its eight-point Gaussian-sum approximation smaller than 2% (see Table 5 of Appendix A.2). The difference between the best-

fit eight-point spectrum and the models of G12, F08, and D11 corresponds to a small $0.5 - 1.5\sigma$ preference for the Gaussian-sum description (column 8). The EBL shapes predicted by S06, KS14, F10, and K10 are disfavored at the $\geq 3 - 6\sigma$ level with respect to our best-fit spectrum. We have not included here the models of Helgason et al. (2012) and Stecker et al. (2012), which estimate the EBL only up to the M ($\sim 5\mu\text{m}$) and I ($\sim 0.8\mu\text{m}$) photometric bands, respectively, and are thus not relevant for most of the TeV spectra listed in Table 2. We note nonetheless that their results are within $1 - 2\sigma$ of the estimates derived in the present work at small wavelengths. Following the approach of the EBL studies by the H.E.S.S. and *Fermi*-LAT collaborations (H.E.S.S. Collaboration 2013f; Ackermann et al. 2012), we estimate the best-fit normalization factor of the EBL models, as listed in column 9.⁴ The best-fit normalizations of the models listed in Table 4 are all larger than 1, though only at the $1 - 2\sigma$ level for the models of G12, F08, D11, and S06. This is not surprising as most of these models were designed to match sets of lower limits based on less complete surveys than the most recent studies, and as such tend to yield lower estimates of the EBL intensity. We compare in Fig. 3 the scaled-up model of G12 with constraints derived from the measurements of H.E.S.S. below $z < 0.2$ and *Fermi*-LAT between $0.5 < z < 1.6$. The H.E.S.S. and *Fermi*-LAT 1σ confidence contours include the statistical and systematic uncertainties on the measurement of the parameter normalizing the model of F08, in the wavelength ranges relevant to these studies (see H.E.S.S. Collaboration 2013f; Biteau 2013). A good agreement on the level of EBL is found between these works and our results.

We investigate more closely the origin of the differences between the gamma-ray based EBL spectrum and the models. Good agreement between our results and all of the models in Table 4 is found below $5\mu\text{m}$. The models of S06, KS14, F10, and KD10 are thus disfavored because of the rather low level of CIB they predict. The models of G12, F08, and D11 tend to predict a level of EBL that is higher than the gamma-ray estimate around $8\mu\text{m}$, while lower around $16\mu\text{m}$. The $\sim 16\mu\text{m}$ point from the gamma-ray data is found to be $\sim 3\sigma_{\text{stat+sys}}$ above the galaxy-count estimate, but the lack of an observation around $8\mu\text{m}$ prevents a direct comparison at this wavelength⁵. These hints of deviations in the $5 - 20\mu\text{m}$ region, which could be indicative of the signature of polycyclic aromatic hydrocarbons, should be taken with caution as neighboring points from the gamma-ray estimates are correlated. Using the covariance matrix shown in Appendix B, the correlation coefficient between the $\sim 8\mu\text{m}$ and $\sim 16\mu\text{m}$ points is negative (-16%), showing that a decrease in the latter would result in an increase of the former, which would considerably reduce the deviations. A firm conclusion on the signature of polycyclic aromatic hydrocarbons cannot be drawn at this stage,

⁴ Renormalizing theoretical or empirical EBL models is not physically motivated, since different components contributing to the spectrum need not scale in the same way. Nonetheless, measuring the best-fit scaling factor for a model is a straightforward way to quantify the model's compatibility with the experimental gamma-ray data.

⁵ A linear interpolation in $\log(\lambda)$ between the 4.5 and $16\mu\text{m}$ points from galaxy counts yields a level of EBL $\sim 3\sigma_{\text{stat+sys}}$ higher than the gamma-ray estimate.

as indicated by the small difference in quality between the model-independent fit of this work and the model-dependent fits (column 2 in Table 4). Increased gamma-

ray statistics from local sources ($z \lesssim 0.1$) and improved constraints from galaxy counts in the $5 - 20 \mu\text{m}$ region would definitely help in deciding the matter.

TABLE 4
TEST STATISTICS OF THE EBL MODELS.

Model	χ^2	ndf	χ^2_γ	χ^2_{EBL}	n_{EBL}	$\sigma(\cdot \neq \text{no EBL})$ ^a	$\sigma(\text{this work} \neq \cdot)$ ^b	α	$\chi^2_\gamma(\alpha)$	$\chi^2_{\text{EBL}}(\alpha)$	$n_{\text{EBL}}(\alpha)$
No EBL	489.1	443	489.1
This work	342.5	442	340.1	2.4	7	11.0
G12	353.5	455	345.2	8.4	12	12.0	0.5	1.13 ± 0.07	346.0	1.9	4
F08	366.1	451	350.2	15.9	9	11.8	1.3	1.05 ± 0.07	352.1	13.6	6
D11	370.0	453	351.0	19.0	10	11.8	1.5	1.16 ± 0.05	356.9	3.5	5
S06	392.7	445	382.0	10.7	3	10.3	5.0	1.18 ± 0.08	380.0	7.5	3
KS14	401.4	456	362.1	39.3	13	11.3	3.0	1.44 ± 0.07	361.2	0.5	4
F10	424.0	449	390.2	33.8	7	9.9	5.7	1.48 ± 0.07	384.6	3.6	3
KD10	433.0	457	366.7	66.3	14	11.1	3.5	1.52 ± 0.14	346.5	0.2	1

^a Significance with which the gamma-ray data prefer the model to the absence of EBL.

^b Significance with which the gamma-ray data prefer the EBL spectrum from this work to the model.

To estimate the total brightness of the EBL, we perform a fit similar to that described above, extending the wavelength range to $0.1 - 1000 \mu\text{m}$ and using twelve points, corresponding roughly to $\Delta_l \sim 0.75$. The fit is underconstrained below $0.25 \mu\text{m}$ and the EBL estimate in the lowest wavelength bin is compatible with zero at the 1σ level. The brightness of the COB in $0.1 - 8 \mu\text{m}$ is estimated to be $36 \pm 11 \text{ nW m}^{-2} \text{ sr}^{-1}$, with a large uncertainty coming from the region $\lambda < 0.25 \mu\text{m}$. Above $105 \mu\text{m}$, the gamma-ray data do not constrain the fit but the CIB is tightly constrained by local measurements, yielding a $8 - 1000 \mu\text{m}$ CIB brightness compatible with that of the COB, with a value of $25.9 \pm 3.4 \text{ nW m}^{-2} \text{ sr}^{-1}$. The total brightness of the EBL is measured with a $\sim 20\%$ accuracy as $62 \pm 12 \text{ nW m}^{-2} \text{ sr}^{-1}$, which is equivalent to $6.5 \pm 1.2\%$ of the brightness of the CMB. This is compatible at the 1σ level with previous estimations based on galaxy counts (Dole et al. 2006) and on models (see e.g. Table 1 in G12, Table 4 in D11, and Table 2 in F10).

We also show in Fig. 3 the best-fit EBL spectrum derived taking into account only the gamma-ray data (light-blue points). A larger binning ($\Delta_l = 1.5$) results because of the loss of information. Gamma-ray data show a spectrum of the EBL from mid-UV up to far IR that is in good agreement with estimates based on galaxy counts. The 11σ deviation from a null EBL intensity and the fact that EBL reconstructed from gamma-ray observations follows the expected spectrum are pieces of evidence against scenarios in which the VHE emission of blazars would primarily come from ultra-high-energy cosmic rays (UHECR) reprocessed along the line of sight (e.g. Essey & Kusenko 2010). Quite a cosmic conspiracy would be needed to explain how secondary gamma rays from UHECR carry the very same imprint as that expected from absorption of primary gamma rays. A more quantitative study of the impact of this process on the EBL reconstruction is left for future work.

To quantify the compatibility between galaxy counts and the four-point EBL spectrum based only on gamma-ray data (light-blue points in Fig. 3), we compute the difference between these estimates in the wavelength range

probed by the gamma-ray data. In order to account for the correlations between the gamma-ray based EBL points as well as for the broadness of the wavelength range including multiple points from galaxy counts, we build the following likelihood for the EBL excess, $\Delta\nu I_\nu$, marginalizing over the EBL parameters and taking into account multiple galaxy counts estimates for a single gamma-ray-based EBL point:

$$\mathcal{L}(\Delta\nu I_\nu) = \int dA \, e^{-\frac{1}{2} \sum_{i \in \text{LL}} \left(\frac{\nu I_\nu(A, \lambda_i) - \nu I_\nu^i - \Delta\nu I_\nu}{\sigma_i^i} \right)^2} \times e^{-\frac{1}{2} [A - A_0]^T V_{A_0}^{-1} [A - A_0]} \quad (24)$$

where A_0 is the vector of the best-fit EBL parameters and where V_{A_0} is their covariance matrix, provided for reference in Appendix B. $\nu I_\nu(\lambda_i)$ and νI_ν^i are the EBL specific intensity based on gamma rays and galaxy counts, respectively. The integration is performed numerically through a Monte Carlo probe of the parameter space within $\pm 3\sigma$ of the best-fit A_0 .

We measure an overall excess $\Delta\nu I_\nu = -0.8 \pm 0.4 \text{ nW m}^{-2} \text{ sr}^{-1}$, with a mild significance at the 2.0σ level based on a likelihood ratio test. The slightly low gamma-ray estimate of the EBL is mostly due to the wavelength range above $25 \mu\text{m}$, with values in the same units of 4.7 ± 2.2 , 1.4 ± 1.4 , -0.4 ± 0.6 , and -0.8 ± 0.3 , in the wavelength ranges $0.26 - 1.2 \mu\text{m}$, $1.2 - 5.2 \mu\text{m}$, $5.2 - 23 \mu\text{m}$, and $23 - 105 \mu\text{m}$, respectively, as shown in Fig. 4. The coarse binning of the EBL spectrum based only on gamma-ray data is possibly responsible for the mildly negative excess, as no tension is observed in the eight-point spectrum when taking into account the local constraints. We note that the model developed for the excess of anisotropy at $1.1 \mu\text{m}$ and $1.6 \mu\text{m}$ detected with CIBER by Zemcov et al. (2014) (see also Kashlinsky et al. 2015, for a critical review), explained as originating from stars stripped from their parent galaxies during mergers, cannot be ruled out by our results given the uncertainties from both approaches. Little room is left for contributions from other unknown populations of sources, especially above $1.2 \mu\text{m}$. This wavelength range is of particular interest for the study of the sources of reionization and we exclude significant contributions from mini-quasars and Pop. III stars as presented e.g. in Cooray & Yoshida (2004). We also exclude more exotic scenar-

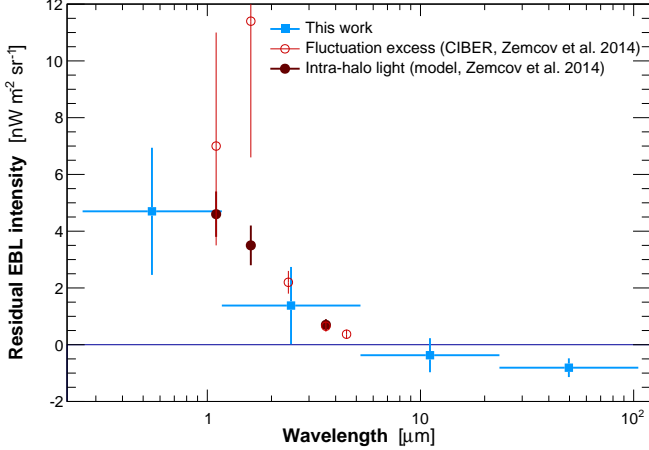


FIG. 4.— Difference between the best-fit EBL spectrum derived from gamma-ray spectra only and the EBL estimates based on galaxy counts (blue squares). The anisotropy excess measured at $1.1\,\mu\text{m}$ and $1.6\,\mu\text{m}$ and a model of the IHL (both from Zemcov et al. 2014) are shown with red-empty and dark-red filled points, respectively.

ios where Pop. III stars would experience a long “Dark Star” phase powered by WIMPs (see in particular Fig. 3 in Maurer et al. 2012).

4.2. Hubble constant

The possibility to constrain the expansion rate of the universe using gamma-ray observation of distant sources was first proposed by Salamon et al. (1994). The idea is rather simple: measurements of the EBL optical depth, τ , are proportional to $\nu I_\nu/H_0$, as shown in Eq. 9, while direct observations provide estimates of the EBL intensity νI_ν , the combination of which thus constrains H_0 .

Such an approach has been pursued e.g. by Barrau et al. (2008) who fixed the EBL intensity within estimates based on galaxy counts. Following a similar approach, we assume here that the EBL intensity can be described by the lower limits in Table 1. This assumption follows the results from Sec. 4.1, showing a rather good agreement between gamma-ray data and galaxy counts.

We hereafter use solely gamma-ray data to estimate $\nu I_\nu/H_0$. Calling H the true value of the Hubble constant and $H_0 = 70\,\text{km s}^{-1}\,\text{Mpc}^{-1}$ the value used to derive the EBL parameters, A_0 , we define the marginalized likelihood over the EBL parameters:

$$\mathcal{L}(H) = \int dA \, e^{-\frac{1}{2} \left[\frac{H_0}{H} A - A_0 \right]^T V_{A_0}^{-1} \left[\frac{H_0}{H} A - A_0 \right]} \times e^{-\frac{\chi_{EBL}^2(A)}{2}} \quad (25)$$

where $\chi_{EBL}^2(A)$ assesses the compatibility of the set of parameters A with local constraints on the EBL, as described in Sec. 3.3.1.

The marginalized likelihood shown in Fig. 5 yields an estimate of $H_0 = 88 \pm 8_{\text{stat}} \pm 13_{\text{sys}}\,\text{km s}^{-1}\,\text{Mpc}^{-1}$. The systematic uncertainty is propagated from the optical depth (7–8%, see Appendix A), with $H_0 \propto 1/\tau$, and then added in quadrature to the bias expected from an excess of intensity with respect to galaxy counts. An offset of $-0.8\,\text{nW m}^{-2}\,\text{sr}^{-1}$, as determined in Sec. 4.1, yields an estimate of the Hubble constant

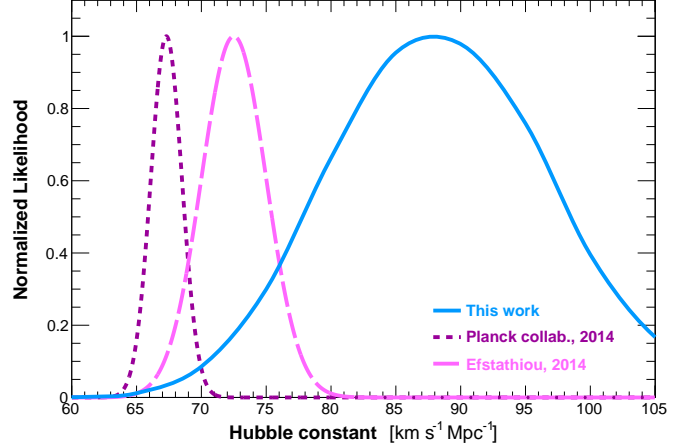


FIG. 5.— Likelihood distribution of the Hubble constant. The estimate based on the comparison of gamma-ray data and local constraints is shown in solid blue. For reference, this estimate is compared to the best-fit values based on CMB observations and the local cosmic distance ladder.

$11\,\text{km s}^{-1}\,\text{Mpc}^{-1}$ lower than the best-fit value. Accounting for both statistical and systematics uncertainties on this measurement, no tension larger than 1.4σ is observed with constraints based on the cosmic distance ladder (Efstathiou 2014) or CMB-based measurements (Planck Collaboration et al. 2014).

Domínguez & Prada (2013) noticed that not only the distance term but also the density of photons used in the optical depth computation could depend on the Hubble constant for a given set of galaxy observations. Within such a formalism, the evolution parameter f_{evol} would be a function of H_0 , with a typical span of $0.5 < f_{\text{evol}} < 2.5$ for $0.5 < H_0/100\,\text{km s}^{-1}\,\text{Mpc}^{-1} < 0.9$ (Domínguez 2015). Marginalizing the likelihood over this range of evolution parameters yields mildly larger uncertainties ($H_0 = 88 \pm 13_{\text{stat}} \pm 13_{\text{sys}}\,\text{km s}^{-1}\,\text{Mpc}^{-1}$), but does not affect our conclusions. We note that the result of Domínguez & Prada (2013), $H_0 = 71^{+4.6}_{-5.6(\text{stat})} {}^{+7.2}_{-13.8(\text{sys})}\,\text{km s}^{-1}\,\text{Mpc}^{-1}$, exploiting the cosmic gamma-ray horizon (Blanch & Martinez 2005) and a fixed EBL spectral shape at $z = 0$ remains the most competitive gamma-ray estimate of the Hubble constant.

4.3. Source redshifts

A similar approach to that devised in Sec. 4.2 can be used to constrain the distance of unknown redshift sources. In the following, we use gamma-ray absorption as a guide for selecting possibly conflicting spectroscopic estimates. We assume a Hubble constant fixed to its nominal value $H_0 = 70\,\text{km s}^{-1}\,\text{Mpc}^{-1}$ and we describe the EBL by its best-fit eight-point spectrum obtained in Sec. 4.1 (combined gamma-ray and local constraints). The best-fit parameters A_0 and covariance matrix V_{A_0} for the eight-parameter spectrum are provided in Appendix B.

We marginalize over the EBL parameters within uncertainties and define the following likelihood for a given

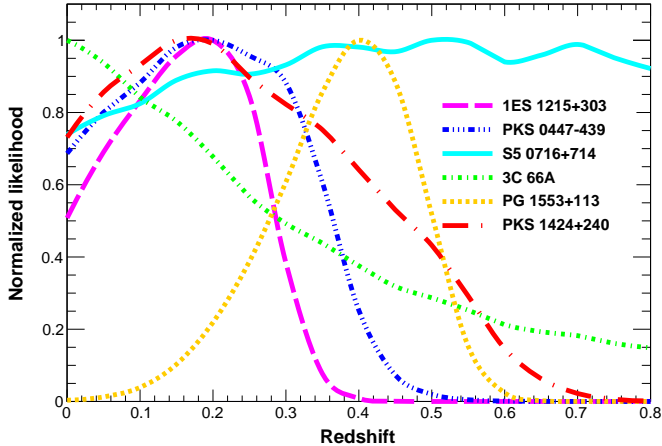


FIG. 6.— Likelihood distribution of the redshift of six TeV blazars. Constraints are obtained after marginalization over the best-fit EBL parameters.

set of spectra from a single source:

$$\mathcal{L}(z) = \int dA e^{-\frac{1}{2}[A-A_0]^T V_{A_0}^{-1}[A-A_0]} \times e^{-\frac{1}{2} \sum (\chi_{\gamma\text{ray points}}^2 + \chi_{\text{HE-VHE}}^2)(A, z)} \quad (26)$$

where the sum is over the spectra of a single source. Note that the spectra used in this sum must be different from the ones used in the estimation of the EBL parameters A_0 , to avoid double counting the same datasets. The unknown-redshift sources are not included in the gamma-ray cosmology sample used to determine A_0 , which justifies our approach. All the intrinsic spectra studied in this section are well matched by intrinsic PWL models.

Six sources with unconstrained distances are listed in Table 2. The likelihood distributions of the redshifts for the six sources are shown in Fig. 6.

- 1ES 1215+303: for which we have gathered two spectra from MAGIC and VERITAS. Two spectroscopic estimates of the redshift of this HBL can be found in the literature: $z = 0.130$ (Bade et al. 1998) and $z = 0.237$ (Lanzetta et al. 1993). Akiyama et al. (2003) show a spectrum and list the redshift as 0.130, but it is not clear whether that redshift is supported by the spectrum or taken from the literature. As shown in Fig. 6, the likelihood profile for this source has a maximum at $z \sim 0.2$. Because this estimate is compatible with zero, we provide an upper limit at the 99% confidence level of $z < 0.35$, and use in the following $z = 0.237$.
- PKS 0447-439: for which we have gathered one spectrum from H.E.S.S. A spectroscopic estimate of $z = 0.205$ was claimed by Perlman et al. (1998), based though on a rather weak feature that was not confirmed by further optical observations (e.g. Pita et al. 2014). Muriel et al. (2015) recently estimated the redshift of this source to be $z = 0.343$, based on the observation of neighbouring galaxies possibly belonging to the

same cluster. The H.E.S.S. spectrum has been used by several teams to constrain the distance of this source, with claimed measurements of $z = 0.16 \pm 0.05$ and $z = 0.20 \pm 0.05$ (Prandini et al. 2012; Zhou et al. 2014, respectively). Such small uncertainties, related to limiting assumptions on the EBL model or on the properties of the intrinsic spectra of TeV blazars, are not confirmed by the H.E.S.S. Collaboration (2013b), which provides an upper limit at the 95% level of $z < 0.59$. Our profile for PKS 0447-439 peaks at $z \sim 0.2$ and we obtain $z < 0.45$ at the 99% confidence level. In the following, we use $z = 0.343$ for this source, noting that $z = 0.205$ yields compatible results given the broadness of the likelihood profile.

- S5 0716+714: for which we have gathered one spectrum from MAGIC. Danforth et al. (2013) detected a system on the line of sight and have also set an upper limit based on the non-detection of lines farther away, constraining the redshift of this IBL within $0.232 \leq z < 0.322$. This range is consistent with the spectroscopy of three galaxies possibly hosted by the same cluster as the source, around $z \sim 0.26$ (Bychkova et al. 2006). In our study, no conclusion can be drawn for S5 0716+714, which shows a very broad maximum around $z \sim 0.5$. In the following, we use the cluster-based $z = 0.26$ as the redshift estimate of this source.
- 3C 66A: for which we have gathered one spectrum from MAGIC. Furniss et al. (2013a) detected an absorber on the line of sight and have constrained the maximum distance of this IBL based on the non-detection of farther lines, finding $0.335 \leq z < 0.41$. Yang & Wang (2010) studied the gamma-ray emission of the object and set an upper limit at $z < 0.58$. For 3C 66A, the likelihood in Fig. 6 peaks at a rather low redshift ($z \sim 0$) and indicates a distance fully compatible with zero within uncertainties. No upper limit on the redshift of 3C 66A can be obtained given the broadness of the distribution. In the following, we use the spectroscopic lower-limit of $z = 0.335$, which is only in mild tension with the likelihood profile (at the 1σ level)
- PG 1553+113: for which we have gathered two spectra from H.E.S.S. and three from MAGIC. Danforth et al. (2010) constrained the redshift of this HBL through spectroscopic observations to $0.433 \leq z < 0.58$, though the lower limit is based on a single line. The authors obtained $z \geq 0.395$ based on more numerous absorbers. Based on gamma-ray observations, Yang & Wang (2010) determined $z < 0.78$. Fixing the EBL absorption to the model of Franceschini et al. (2008), the H.E.S.S. collaboration (Abramowski et al. 2015) measured $z = 0.49 \pm 0.04$, or $z < 0.56$ at the 95% confidence level, compared to $z < 0.60$ and

$z < 0.62$ from the MAGIC and VERITAS collaborations, respectively (MAGIC Collaboration et al. 2014; Aliu et al. 2015). Our study accounts for the uncertainties on the EBL and thus yields a more conservative gamma-ray estimate of the redshift of this source, with most likely value $z = 0.41^{+0.08}_{-0.11}$, preferred at the 3.4σ level to a null redshift. For comparison with the work of Abramowski et al. (2015), we obtain a 95% upper-limit on the redshift of the source $z < 0.53$ ($z < 0.58$ at 99%). In the following, we set the redshift of PG 1553+113 to $z = 0.433$.

- PKS 1424+240: for which we have gathered three spectra from VERITAS and three from MAGIC. Furniss et al. (2013b) determined a spectroscopic lower limit on the redshift of this object, $z \geq 0.604$. Prandini et al. (2011) claim a measurement of $z = 0.24 \pm 0.05$, with small uncertainties coming from the same limiting assumptions as for PKS 0447-439. Yang & Wang (2010) provide a more robust upper-limit at $z < 1.19$. As for 3C 66A, the likelihood profile for PKS 1424+240 is fully compatible with zero redshift, but an upper limit can be set at $z < 0.64$ at the 99% confidence level. In the following, we use the spectroscopic lower-limit of $z = 0.604$, which is in slight tension (2.4σ) with the likelihood profile.

The four constraints on redshifts derived in this section are the most stringent gamma-ray upper limits to date for these sources.

4.4. Axion-like particles

With a best-fit EBL spectrum at hand and redshift estimates for all sources, we can search for any significant residual, which might be indicative of new physics. Though we restricted the study to a gamma-ray cosmology sample of spectra for the determination of the EBL and of the Hubble constant, we study here all the spectra listed in Table 2, with spectral models provided in column 5.

We investigate in this section deviations from classical absorption resulting from coupling of gamma rays with axion-like particles. Gamma rays from blazars could convert into such hypothetical particles (cousins of the QCD axion with free mass and coupling) and could then convert back into gamma rays within the Galactic magnetic field. Several locations have been studied for the initial conversion, be it within the magnetic field of the emission region, in the vicinity of the source (host, jet galaxy, cluster) or in the intergalactic medium (see e.g. Hooper & Serpico 2007; de Angelis et al. 2007; Sánchez-Conde et al. 2009; Tavecchio et al. 2012). An observable effect would be a gamma-ray spectral hardening at the highest optical depth, which has been weakly observed by several analyses (Domínguez et al. 2011a; Horns & Meyer 2012; Meyer et al. 2013; Rubtsov & Troitsky 2014). We note nonetheless that a large fraction of the parameter space corresponding to these hints has been excluded by Abramowski et al. (2013) using the lack of point-to-point fluctuations in the spectrum of the bright blazar PKS 2155-304.

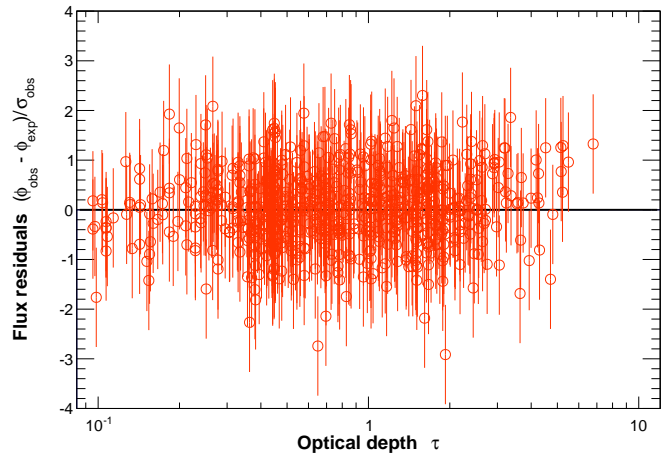


FIG. 7.— Residuals to the best-fit models for the 106 spectra (737 points) studied in this paper, as a function of optical depth.

The spectral points and best-fit models are shown in Appendix C. We show in Fig. 7 the residuals to the best-fit models as a function of optical depth for these 737 points. All of the spectra are well represented by our models. The residuals are scattered around an average of 0.05 ± 0.03 with an rms of 0.73 ± 0.02 and are well represented by a normal distribution, with a p value of 22% following an Anderson-Darling test. The rms is significantly smaller than 1, which is consistent with the small χ^2 found in Sec. 4.1.

In the following, we search for a hardening of the TeV spectra at the highest optical depths as in Horns & Meyer (2012), while leaving model-dependent constraints on the axion-like particles' coupling to gamma rays to future studies. Horns & Meyer (2012) model a sample of 50 spectra and assume an EBL intensity fixed to the model of Kneiske & Dole (2010). Noting an rms of the flux residuals smaller than one, and deviations from a normal distribution based on an Anderson-Darling test, Horns & Meyer (2012) chose to ignore uncertainties on the data and to study the following quantity:

$$R = \frac{\phi_i - \phi_{\text{model},i}}{\phi_i + \phi_{\text{model},i}} \quad (27)$$

where ϕ_i is the observed flux for the point i and $\phi_{\text{model},i}$ is the expected flux resulting from the model.

Comparing the distribution of R in a reference sample composed of points at $1 < \tau \leq 2$ and in a search sample at $\tau > 2$, the authors find a 4.2σ discrepancy, with an average value of $R \sim 0.25$ at large optical depth (estimated from the cumulative distribution function shown in Fig. 3 of their publication). Defining the flux-enhancement factor as $FE = \phi/\phi_{\text{model}}$, the flux of TeV blazars would then exceed the expectations by $FE = (1 + R)/(1 - R) \sim 1.7$ above an optical depth of $\tau > 2$. They explain this $\sim 70\%$ increase in flux as an hint for mixing of gamma rays with axion-like particles. Performing the same test with our best-fit EBL spectrum and our larger dataset, we find a slightly larger discrepancy of 4.5σ , for an average $R \sim 0.1$. However, we argue in the following that this test is flawed, because it neglects the uncertainties on the measured flux.

We measure the average flux enhancement FE in var-

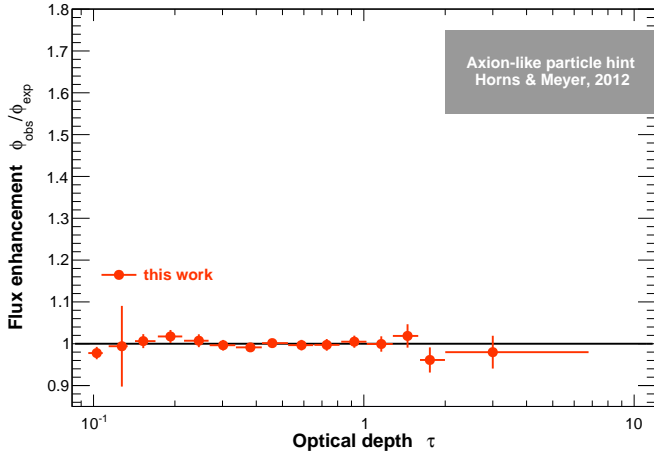


FIG. 8.— Flux enhancement, defined by the ratio of observed and expected fluxes, as a function optical depth. The shaded gray region is the flux enhancement implied by the results of Horns & Meyer (2012).

ious optical-depth bins, using a sample of gamma-ray spectra twice as large as any other studied. The residuals show a normal distribution, whose parameters are largely independent of redshift, energy, and optical depth. We thus include the uncertainties in the computation of the flux enhancement, weighting the relative contributions of the spectral points, as:

$$FE = \left\langle \frac{\phi}{\phi_{\text{model}}} \right\rangle_i = \frac{\sum_i \phi_i \phi_{\text{model},i} / \sigma_{\phi,i}^2}{\sum_i \phi_{\text{model},i}^2 / \sigma_{\phi,i}^2} \quad (28)$$

which is the usual χ^2 -based weighted average, propagating the uncertainty on the observed flux $\sigma_{\phi,i}$. Note that scaling the uncertainties on the observed flux up or down affects the errors on the flux enhancement estimate, but not the mean.

The flux enhancement is shown as a function of optical depth in Fig. 8. The 106 spectra constrain the flux enhancement at optical depths larger than $\tau > 2$ to $FE = 0.98 \pm 0.04$, for an average optical depth $\tau = 3.0$. This value, consistent with 1, shows no deviation from expectations. A flux enhancement of more than $\sim 40\%$ is excluded beyond the 5σ level, taking only statistical uncertainties into account. Even assuming a systematic bias of 10% at large optical depth (see Appendix A), the flux enhancement corresponding to the results of Horns & Meyer (2012) (gray shaded region in Fig. 8) remains excluded at the 5σ level.

Applying the statistical test of Horns & Meyer (2012) to our dataset with our EBL spectrum therefore shows a more significant effect (4.5σ compared to 4.2), albeit with smaller amplitude than they observe ($R \sim 0.1$ compared to ~ 0.25). However, we find little indication that the uncertainties on the individual flux measurements are unreliable, and when they are taken into account, we do not find a flux enhancement at large optical depths. The highest flux enhancements at optical depth above 2 in the sample studied here are obtained for the last points of the spectra of 1ES 1959+650 (Whipple, 2002), at $\tau = 5.2$,

3C 279 (MAGIC, 2006), at $\tau = 4.2$, and 1ES 0229+200 (H.E.S.S., 2005-2006), at $\tau = 6.7$. They show flux enhancement of 13, 14 and even 23, respectively, but with uncertainties on the order of 100% that strongly bias the test devised by Horns & Meyer (2012). The most likely source of anomaly seen by these authors seems then to be the choice of statistical test rather than a specific dataset (their set of spectra is to a large extent included in Table 2). We note that Meyer et al. (2013) studied the residuals normalized to uncertainties, as shown in Fig. 7, and found an average flux enhancement significant at the 4.4σ level based on a t test and using the EBL model of Kneiske & Dole (2010). Performing the same test with our sample yields a significance of 1.1σ for the model of Kneiske & Dole (2010) and 2.6σ for the EBL spectrum derived in Sec. 4.1. The slightly different response of this test with respect to that shown in Fig. 8 is possibly due to the weighting of the points in the averaging process ($\propto 1/\sigma_{\phi,i}$ for the t test and $\propto 1/\sigma_{\phi,i}^2$ for a χ^2 -based average in Eq. 28).

We conclude, based on the largest gamma-ray sample studied so far, that current VHE gamma-ray observations do not show a detectable flux enhancement at large optical depths and find little motivation for a lower limit on the coupling of axion-like particles with photons as reported in Meyer et al. (2013).

4.5. Lorentz invariance violation

We investigate in this section the compatibility of the 86 spectra in the gamma-ray cosmology sample with a quantum-gravity induced effect such as proposed by Kifune (1999); Aloisio et al. (2000); Protheroe & Meyer (2000); Ellis et al. (2001); Amelino-Camelia & Piran (2001); Stecker & Glashow (2001). These authors conducted their investigations following the publication of the spectrum of Markarian 501 observed by HEGRA in 1997 (Aharonian et al. 1999), but the limited constraints on the EBL and on blazars' spectra, which were only a handful in 2000, prevented a quantitative constraint. This spectrum is not included in our study because it was updated in Aharonian et al. (2001).

We model the effect of a Lorentz invariance violation (LIV) adopting the formalism of Jacob & Piran (2008). The starting point consists in a leading-order modification of the special relativistic relation $E^2 = p^2 c^2 + m^2 c^4$, where E and p are the energy and momentum of a particle of mass m . The effect should become significant around a quantum-gravity energy scale E_{QG} , a correction of order $n = 1, 2$ yielding:

$$E^2 = p^2 c^2 + m^2 c^4 \pm E^2 \left(\frac{E}{E_{\text{QG}}} \right)^n \quad (29)$$

so that the norm of the momentum four-vector, $E^2 - p^2 c^2$, is not a Lorentz invariant any more.

Equation 29 alters the kinematics of electron-positron pair creation, as in the collision of a TeV gamma ray interacting with an EBL photon. One needs to modify the special-relativistic threshold $\epsilon_{\text{thr}} > m_e^2 c^4 / E$, with m_e the mass of the electron and where ϵ and E are the energy of the two photons. The original spectrum of Markarian 501 published by HEGRA hinted at a gamma-ray absorption lower than predicted by classical interaction with the EBL, which corresponds to the subluminal case

("−" correction in Eq. 29) that we study in the following. A superluminal correction ("+" in Eq. 29) would yield either a lower threshold and pair creation on the CMB (Jacob & Piran 2008) or photon decay if the dynamics are favorable (e.g. Shao & Ma 2010), in which cases the absorption would be larger than classical. The investigation of the superluminal scenario, possibly requiring assumptions on the dynamics of the process, is left for future studies.

In the subluminal case, the energy-momentum conservation yields the modified pair-creation threshold:

$$\epsilon_{thr} = \frac{m_e^2 c^4}{E} + \frac{1 - 2^{-n}}{4} \left(\frac{E}{E_{QG}} \right)^n E \quad (30)$$

if Eq. 29 is applied to the photons and leptons. The term $1 - 2^{-n}$ should be replaced by 1 if only the photons are affected, which is equivalent to considering a quantum-gravity energy scale twice as large for $n = 1$. One can rewrite Eq. 30 as:

$$\epsilon_{thr} = \frac{m_e^2 c^4}{E} \times \left[1 + \left(\frac{E}{E_{\gamma, LIV}} \right)^{n+2} \right] \quad (31)$$

where

$$\begin{aligned} E_{\gamma, LIV} &= [(2m_e c^2)^2 E_{QG}^n / (1 - 2^{-n})]^{1/(n+2)} \\ &= 29.4 \text{ TeV} \times \left(\frac{E_{QG}}{E_{\text{Planck}}} \right)^{1/3}, \text{ for } n = 1 \end{aligned} \quad (32)$$

with $E_{\text{Planck}} = \sqrt{\hbar c^5 / G} = 1.22 \times 10^{28} \text{ eV}$. A leading quadratic correction, $n = 2$, yields $E_{\gamma, LIV} = 120 \text{ PeV} \times \sqrt{E_{QG} / E_{\text{Planck}}}$, out of reach of current experiments for $E_{QG} \sim E_{\text{Planck}}$. We focus in the following on the linear case, $n = 1$, but we derive the modified EBL optical depth in the general case as:

$$\begin{aligned} \tau(E_0, z_0) &= \frac{3}{4} \frac{\sigma_T c}{H_0} \int_0^{z_0} dz \frac{\partial l}{\partial z}(z) \int_0^\infty d\epsilon \frac{\partial n}{\partial \epsilon}(\epsilon, z) \\ &\quad \left(\frac{\epsilon_{thr}}{\epsilon} \right)^2 P \left(\sqrt{1 - \frac{\epsilon_{thr}}{\epsilon}} \right) \end{aligned} \quad (33)$$

where we follow the notations of Sec. 2.

Assuming that the energy and redshift dependences of the EBL photon field can be decoupled and using the same changes of variable as in Sec. 2, the LIV-affected EBL optical depth can be expressed as:

$$\begin{aligned} \tau(E_0, z_0) &= \frac{3\pi\sigma_T}{H_0} \times \frac{E_0}{m_e^2 c^4} \times \int_{-\infty}^\infty de_0 \exp(-3e_0) \\ &\quad \times \nu I_\nu \left(e_0 - \ln \frac{E_0}{m_e c^2} \right) \int_0^{z_0} dz \frac{\partial l}{\partial z} \frac{evol(z)}{(1+z)^4} \\ &\quad \times \left[1 + \left(\frac{(1+z)E_0}{E_{\gamma, LIV}} \right)^{n+2} \right] P(\beta_{\max}) \end{aligned} \quad (34)$$

where

$$\beta_{\max}^2 = 1 - \frac{\exp(-e_0)}{(1+z)^2} \left[1 + \left(\frac{(1+z)E_0}{E_{\gamma, LIV}} \right)^{n+2} \right] \quad (35)$$

We compare the LIV-affected optical depth to the classical one in Fig. 9, using the eight-point specific intensity

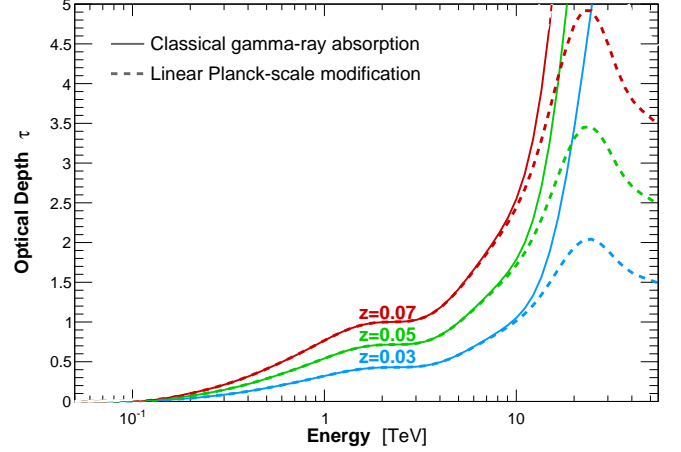


FIG. 9.— EBL optical depth at three redshifts, in the classical case (solid lines) and in the case of a LIV modification at the Planck scale (dashed lines).

of the EBL obtained in Sec. 4.1. The main effect of LIV on gamma-ray absorption is a reduction of the optical depth above 10 TeV, largely independent of redshift.

The approach developed in Sec. 3.3 consists in finding the best EBL spectrum jointly accounting for the absorption signature seen in gamma rays and for local constraints on the EBL. We add here an extra free parameter that is the energy scale E_{QG} at which LIV modifications of the pair-creation threshold take place. We vary E_{QG} and compute the best-fit χ^2 accounting for both gamma-ray spectra and local constraints on the EBL. We define the test statistic $TS = \chi^2(E_{QG}, A_{QG}) - \chi^2(\infty, A_\infty)$, where the latter χ^2 is measured at the best-fit EBL level in the classical case, and where A denotes the EBL parameters, left free to vary for each quantum-gravity scale.

Figure 10 shows the likelihood profile, $\mathcal{L} = \exp(-TS/2)$, as a function of the inverse of E_{QG} normalized to the Planck energy. Interestingly, a slight excess can be seen around the the Planck scale, though with a significance of only 2.4σ . Our study is performed using a sample of 86 spectra that includes the very observation of Markarian 501 by HEGRA that triggered substantial theoretical developments on modifications of the pair-creation threshold. The original spectrum, which covers the energy range $0.56 - 22 \text{ TeV}$, was reported in Aharonian et al. (1999). The data were subsequently re-analyzed by Aharonian et al. (2001) with an improved energy resolution, yielding a compatible spectrum covering the energy range $3.3 - 21 \text{ TeV}$, which is the spectrum included in our gamma-ray cosmology sample. Using instead the original spectrum enhances the Planck-scale excess to the 4σ level. The smaller energy coverage of the higher-resolution spectrum results in a less constrained intrinsic emission and the observed spectrum has a somewhat sharper rollover at the highest energies, explaining the decrease in significance from 4σ down to 2.4σ . Given the low significance of the excess, we provide lower limits on the quantum-gravity energy scale of $E_{QG} > 0.78 \times E_{\text{Planck}}$ (95%) and $E_{QG} > 0.65 \times E_{\text{Planck}}$ (99%). A 10% systematic uncertainty on the energy scale of gamma-ray instruments similarly impacts the quantum-gravity energy estimate, and we quote a robust

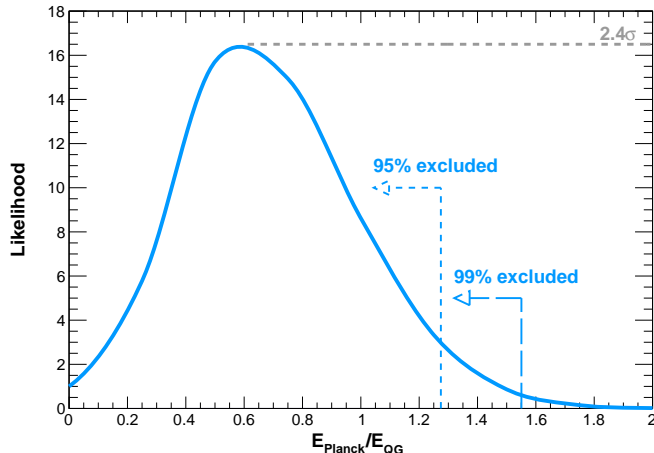


FIG. 10.— Likelihood profile of the quantum-gravity energy scale, leaving the eight-point EBL spectrum free.

lower limit accounting for the systematic uncertainties of $E_{QG} > 0.6 \times E_{\text{Planck}}$.

Other constraints on LIV have been derived from observations of high-energy sources. The synchrotron emission by electrons in the Crab nebula has been used, e.g. by Jacobson et al. (2003), to constrain a linear subluminal term (the same as constrained here) to a quantum gravity scale seven orders of magnitude above the Planck scale. Some authors nonetheless argue that this test is not only kinematics but also depends on the dynamics of process, which are far from being understood within quantum-gravity phenomenology (Amelino-Camelia 2013). A suppressed cross section would then mitigate the constraints from the Crab nebula. A more pristine test comes from observations of gamma-ray bursts (GRBs) by *Fermi*, assuming that LIV affects the propagation time of photons in an energy-dependent way. The most recent constraints have been derived by Vasileiou et al. (2013) who obtain, after taking into account possible internal delays in the source, a lower limit $E_{QG} \geq 2 \times E_{\text{Planck}}$ from a single GRB (090510), and $E_{QG} \geq 0.1 \times E_{\text{Planck}}$ from three others.

One could conclude from the GRB 090510 limit that any modification of the pair-creation threshold is ruled out up to $2 \times E_{\text{Planck}}$, but this would be overlooking the fact that time-delay and absorption observations constrain two different processes. The underlying theory might indeed preserve the speed of light, not impacting time delay observations, but at the same time affect the dispersion relation of particles, leaving an imprint in blazars' spectra (i.e. $v = \partial E / \partial p$ would no longer be valid, see Amelino-Camelia 2013). High-statistics observations above 10 TeV will be required to further study quantum-gravity effects, and the formalism we have developed in this section will prove useful to further constrain LIV with gamma-ray observations of blazars.

5. CONCLUSIONS

A wealth of data has been published by ground-based gamma-ray observatories over the past two decades. We have compiled the most extensive set of gamma-ray spectra from VHE blazars to date, with 106 spectra from 38 objects, corresponding to a total of about 300,000 gamma

rays. This is twice the size of any sample studied before.

Our first result is purely analytical. We have discovered that the triple integral relating the gamma-ray optical depth to the EBL intensity can be reduced to a double integral without any loss of generality. We have further shown that, assuming a decoupling of the evolution of the EBL and of its rest-frame spectrum, the gamma-ray optical depth is the convolution of the EBL intensity with the EBL kernel.

This analytical work significantly reduces the complexity of the spectral reconstruction of the EBL based on gamma-ray observations. The decoupling approximation introduces rather small ($\lesssim 5\%$) systematic errors for sources in the local universe. Using a joint spectral analysis of a subsample of 86 spectra, we deconvolve the intrinsic emission of the sources from the imprint of the EBL spectrum. The reconstructed EBL intensity is preferred at the 11σ level to the absence of gamma-ray absorption, and we reconstruct an eight-point spectrum covering the wavelength range $0.26 - 105 \mu\text{m}$, from mid-UV to far IR. The spectrum of the EBL based on gamma-ray observations is in good agreement with estimates based on galaxy counts, with uncertainties that leave some room for contributions from e.g. intra-halo light (Zemcov et al. 2014), while constraining the emission of reionization sources such as Pop. III stars or miniquasars. The brightnesses of the COB and CIB are measured to be $36 \pm 11 \text{ nW m}^{-2} \text{ sr}^{-1}$ and $25.9 \pm 3.4 \text{ nW m}^{-2} \text{ sr}^{-1}$, respectively. Once integrated between $0.1 - 1000 \mu\text{m}$, the EBL is 6.5 % of the CMB, with an overall uncertainty on this number of 20 %.

Our third result is a gamma-ray measurement of the Hubble constant, $H_0 = 88 \pm 8_{\text{stat}} \pm 13_{\text{sys}} \text{ km s}^{-1} \text{ Mpc}^{-1}$, that is both model independent and based on a significant number of gamma-ray spectra. Such constraints on the expansion rate of the universe are independent from measurements based on the CMB and the cosmic ladder of distances.

We measure no significant flux enhancement at large optical depths and we rule out at the 5σ level the “pair-production anomaly” as obtained by Horns & Meyer (2012). This suggests that the level of mixing of axion-like particles with TeV photons, if any, is below previous estimates based on this effect. We would also like to correct two misconceptions sometimes circulating in the literature. (i) The best-fit EBL spectrum based on gamma-ray observations is not significantly lower than the minimum EBL level. (ii) The intrinsic gamma-ray spectra reconstructed after deabsorption from the EBL effect are not too hard with respect to expectations. All the intrinsic spectra in our fits are softer than measured at lower energy when contemporaneous data are available. This diminishes the motivation for scenarios where axion-like particles impact gamma-ray absorption, or where secondaries from UHECR contribute to the gamma-ray signal observed on Earth.

Finally, we constrain the impact of a Lorentz invariance violation on gamma-ray absorption. A modified dispersion relation, with a correction scaling as the ratio of the gamma-ray energy and the Planck energy, alters the threshold of pair creation and results in milder absorption of $> 10 \text{ TeV}$ gamma rays from blazars. Our formalism takes into account both the spectrum and the evolution of the EBL. It also enables a quantitative anal-

ysis of blazars' spectra in the presence of LIV. A weak 2.4σ excess prevents us from ruling out a modification at the Planck energy, but we rule out for the first time any effect below $0.6 \times E_{\text{Planck}}$ at the 99% confidence level.

The successes of gamma-ray cosmology (see Biteau 2013, for a review) are far from being closed by this work. Major progress in UV and IR observations of distant galaxies has been achieved in recent years, in particular with Galex, Spitzer, and Herschel. Further achievements are expected from the James Webb Space Telescope (JWST, Gardner et al. 2006) during the next decade between 0.6 and $27\mu\text{m}$, with improved constraints from galaxy counts in the optical and mid-IR. The combination of next-generation local constraints with the tremendous gamma-ray sensitivity of the Cherenkov Telescope Array (CTA, Acharya et al. 2013) above 30 GeV could significantly refine the binning of the EBL spectrum. The theoretical limit is dictated by the energy resolution of gamma-ray telescopes, about 10% in gamma-ray energy or equivalently 10% in EBL wavelength. Such fine spectroscopy could clearly show spectral signatures from polycyclic aromatic hydrocarbons, from intra-halo light, or from the sources of the reionization of the universe. The combined constraints of CTA and JWST will also be crucial for the measurement of the Hubble constant based on gamma-ray absorption.

Further developments of analyses at the event level (binned or unbinned), such as 3ML or GammaLib (Knödlseeder 2013), combined with full likelihood spectral techniques such as developed in Piron et al. (2001), could increase the statistical power of the approach developed

in this paper. Such methods are in principle not affected by overestimated uncertainties from published spectra, where correlations are neglected, and would open the possibility of a broad-band spectral fit, e.g. combining the data from *Fermi*-LAT, Cherenkov telescopes, and HAWC (Abeysekara et al. 2013). The subfield of gamma-ray cosmology focusing on the fate of the pairs produced by gamma-ray absorption, and how they could be impacted by the intergalactic magnetic field (see Durrer & Neronov 2013; Chen et al. 2014), will greatly benefit from these ongoing developments. Finally, we are working on the extension of the method that we have presented here to higher redshifts ($z > 1$), where a simple parametrization of the EBL evolution starts to fail. If successful, significant improvements in the spectrum of the EBL below $1\mu\text{m}$ can be expected from the analysis of *Fermi*-LAT blazars.

We would like to thank the corresponding authors of the many papers listed in Table 2 for providing the data points corresponding to their published results. We thank the referee whose work significantly benefited this paper. We would also like to thank Joel Primack, Michael Dine, Stefano Profumo, Alberto Dominguez, Matthieu Bethermin, and Abelardo Moralejo for valuable discussions about this work, Amy Furniss for helping in the collection of the VERITAS spectra, and Steve Fegan for suggesting the use of a Gaussian-sum model for the EBL spectrum. We gratefully acknowledge support from the U.S. National Science Foundation award PHY-1229792.

REFERENCES

- Abdo, A. A., et al. 2010, *ApJ*, 710, 1271
—, 2011, *ApJ*, 727, 129
Abeysekara, A. U., et al. 2013, *Astroparticle Physics*, 50, 26
Abramowski, A., et al. 2013, *Phys. Rev. D*, 88, 102003
—, 2015, *ApJ*, 802, 65
Acciari, V., et al. 2009a, *ApJ*, 690, L126
Acciari, V. A., et al. 2008, *ApJ*, 684, L73
—, 2009b, *ApJ*, 695, 1370
—, 2010a, *ApJ*, 709, L163
—, 2010b, *ApJ*, 715, L49
—, 2011a, *ApJ*, 738, 169
—, 2011b, *ApJ*, 738, 25
Acharya, B. S., et al. 2013, *Astroparticle Physics*, 43, 3
Ackermann, M., et al. 2012, *Science*, 338, 1190
Aharonian, F., et al. 2002, *A&A*, 393, 89
—, 2003a, *A&A*, 406, L9
—, 2003b, *A&A*, 403, 523
—, 2005a, *A&A*, 430, 865
—, 2005b, *A&A*, 442, 895
—, 2005c, *A&A*, 437, 95
—, 2007a, *A&A*, 470, 475
—, 2007b, *A&A*, 473, L25
—, 2007c, *A&A*, 475, L9
—, 2008a, *A&A*, 481, L103
—, 2008b, *A&A*, 477, 481
—, 2009, *ApJ*, 696, L150
Aharonian, F. A., et al. 1999, *A&A*, 349, 11
—, 2001, *A&A*, 366, 62
Akiyama, M., Ueda, Y., Ohta, K., Takahashi, T., & Yamada, T. 2003, *ApJS*, 148, 275
Albert, J., et al. 2006, *ApJ*, 648, L105
—, 2007a, *ApJ*, 666, L17
—, 2007b, *ApJ*, 667, L21
—, 2007c, *ApJ*, 662, 892
—, 2007d, *ApJ*, 663, 125
Aleksić, J., et al. 2010, *A&A*, 519, A32
—, 2011a, *ApJ*, 730, L8
—, 2011b, *ApJ*, 726, 58
—, 2012a, *A&A*, 539, A118
—, 2012b, *A&A*, 544, A142
—, 2012c, *A&A*, 544, A75
—, 2012d, *ApJ*, 748, 46
—, 2013, *A&A*, 556, A67
—, 2014a, *A&A*, 567, A135
—, 2014b, *A&A*, 563, A91
Aliu, E., et al. 2011, *ApJ*, 742, 127
—, 2012a, *ApJ*, 750, 94
—, 2012b, *ApJ*, 755, 118
—, 2013a, *ApJ*, 779, 92
—, 2013b, *ApJ*, 775, 3
—, 2014, *ApJ*, 782, 13
—, 2015, *ApJ*, 799, 7
Aloisio, R., Blasi, P., Ghia, P. L., & Grillo, A. F. 2000, *Phys. Rev. D*, 62, 053010
Amelino-Camelia, G. 2013, *Living Reviews in Relativity*, 16, 5
Amelino-Camelia, G., & Piran, T. 2001, *Phys. Rev. D*, 64, 036005
Amenomori, M., et al. 2003, *ApJ*, 598, 242
Anderhub, H., et al. 2009a, *ApJ*, 704, L129
—, 2009b, *ApJ*, 705, 1624
Archambault, S., et al. 2013, *ApJ*, 776, 69
—, 2014, *ApJ*, 785, L16
Arendt, R. G., & Dwek, E. 2003, *ApJ*, 585, 305
Arlen, T., et al. 2013, *ApJ*, 762, 92
Ashby, M. L. N., et al. 2013, *ApJ*, 769, 80
Bade, N., Beckmann, V., Douglas, N. G., Barthel, P. D., Engels, D., Cordis, L., Nass, P., & Voges, W. 1998, *A&A*, 334, 459
Barrau, A., Gorecki, A., & Grain, J. 2008, *MNRAS*, 389, 919
Bartoli, B., et al. 2011, *ApJ*, 734, 110
—, 2012, *ApJ*, 758, 2
Bernstein, R. A. 2007, *ApJ*, 666, 663
Berta, S., et al. 2011, *A&A*, 532, A49
B  thermin, M., Dole, H., Beelen, A., & Aussel, H. 2010, *A&A*, 512, A78
B  thermin, M., et al. 2012, *A&A*, 542, A58
Biteau, J. 2013, in *SF2A-2013: Proceedings of the Annual meeting of the French Society of Astronomy and Astrophysics*, ed. L. Cambresy, F. Martins, E. Nuss, & A. Palacios, 303–312
Blanch, O., & Martinez, M. 2005, *Astroparticle Physics*, 23, 608
Bychkova, V. S., Kardashev, N. S., Boldycheva, A. V., Gnedin, Y. N., & Maslennikov, K. L. 2006, *Astronomy Reports*, 50, 802
Chandra, P., et al. 2010, *Journal of Physics G Nuclear Physics*, 37, 125201

- . 2012, *Journal of Physics G Nuclear Physics*, 39, 045201
- Chen, W., Buckley, J. H., & Ferrer, F. 2014, arXiv:1410.7717
- Cooray, A., & Yoshida, N. 2004, *MNRAS*, 351, L71
- Danforth, C. W., Keeney, B. A., Stocke, J. T., Shull, J. M., & Yao, Y. 2010, *ApJ*, 720, 976
- Danforth, C. W., Nalewajko, K., France, K., & Keeney, B. A. 2013, *ApJ*, 764, 57
- Daniel, M. K., et al. 2005, *ApJ*, 621, 181
- de Angelis, A., Roncadelli, M., & Mansutti, O. 2007, *Phys. Rev. D*, 76, 121301
- Dole, H., et al. 2006, *A&A*, 451, 417
- Domínguez, A. 2015, private communication
- Domínguez, A., Finke, J. D., Prada, F., Primack, J. R., Kitaura, F. S., Siana, B., & Paneque, D. 2013, *ApJ*, 770, 77
- Domínguez, A., & Prada, F. 2013, *ApJ*, 771, L34
- Domínguez, A., Sánchez-Conde, M. A., & Prada, F. 2011a, *J. Cosmology Astropart. Phys.*, 11, 20
- Domínguez, A., et al. 2011b, *MNRAS*, 410, 2556
- Dube, R. R., Wickes, W. C., & Wilkinson, D. T. 1979, *ApJ*, 232, 333
- Durrer, R., & Neronov, A. 2013, *A&A Rev.*, 21, 62
- Dwek, E., & Krennrich, F. 2013, *Astroparticle Physics*, 43, 112
- Efstathiou, G. 2014, *MNRAS*, 440, 1138
- Ellis, J., Mavromatos, N. E., & Nanopoulos, D. V. 2001, *Phys. Rev. D*, 63, 124025
- Essey, W., & Kusenko, A. 2010, *Astroparticle Physics*, 33, 81
- Finkbeiner, D. P., Davis, M., & Schlegel, D. J. 2000, *ApJ*, 544, 81
- Finke, J. D., Razzaque, S., & Dermer, C. D. 2010, *ApJ*, 712, 238
- Fixsen, D. J., Dwek, E., Mather, J. C., Bennett, C. L., & Shafer, R. A. 1998, *ApJ*, 508, 123
- Franceschini, A., Rodighiero, G., & Vaccari, M. 2008, *A&A*, 487, 837
- Furniss, A., Fumagalli, M., Danforth, C., Williams, D. A., & Prochaska, J. X. 2013a, *ApJ*, 766, 35
- Furniss, A., et al. 2013b, *ApJ*, 768, L31
- Gardner, J. P., Brown, T. M., & Ferguson, H. C. 2000, *ApJ*, 542, L79
- Gardner, J. P., et al. 2006, *Space Sci. Rev.*, 123, 485
- Georganopoulos, M., Finke, J. D., & Reyes, L. C. 2010, *ApJ*, 714, L157
- Ghisellini, G., Celotti, A., Fossati, G., Maraschi, L., & Comastri, A. 1998, *MNRAS*, 301, 451
- Gilmore, R. C., Somerville, R. S., Primack, J. R., & Domínguez, A. 2012, *MNRAS*, 422, 3189
- Godambe, S. V., et al. 2008, *Journal of Physics G Nuclear Physics*, 35, 065202
- Gould, R. J., & Schröder, G. P. 1967a, *Physical Review*, 155, 1404
- . 1967b, *Physical Review*, 155, 1408
- Helgason, K., Ricotti, M., & Kashlinsky, A. 2012, *ApJ*, 752, 113
- H.E.S.S. Collaboration. 2010a, *A&A*, 516, A56
- . 2010b, *A&A*, 511, A52
- . 2010c, *A&A*, 520, A83
- . 2012a, *A&A*, 539, A149
- . 2012b, *A&A*, 538, A103
- . 2012c, *A&A*, 542, A94
- . 2013a, *A&A*, 554, A72
- . 2013b, *A&A*, 552, A118
- . 2013c, *A&A*, 559, A136
- . 2013d, *MNRAS*, 434, 1889
- . 2013e, *A&A*, 554, A107
- . 2013f, *A&A*, 550, A4
- Hooper, D., & Serpico, P. D. 2007, *Physical Review Letters*, 99, 231102
- Hopwood, R., et al. 2010, *ApJ*, 716, L45
- Horns, D., & Meyer, M. 2012, *J. Cosmology Astropart. Phys.*, 2, 33
- Jacob, U., & Piran, T. 2008, *Phys. Rev. D*, 78, 124010
- Jacobson, T., Liberati, S., & Mattingly, D. 2003, *Nature*, 424, 1019
- Kashlinsky, A., Mather, J. C., Helgason, K., Arendt, R. G., Bromm, V., & Moseley, S. H. 2015, *ApJ*, 804, 99
- Keenan, R. C., Barger, A. J., Cowie, L. L., & Wang, W.-H. 2010, *ApJ*, 723, 40
- Khaire, V., & Srianand, R. 2015, *ApJ*, 805, 33
- Kifune, T. 1999, *ApJ*, 518, L21
- Kneiske, T. M., & Dole, H. 2010, *A&A*, 515, A19
- Knödseder, J. 2013, arXiv:1307.5560
- Lanzetta, K. M., Turnshek, D. A., & Sandoval, J. 1993, *ApJS*, 84, 109
- Levenson, L. R., Wright, E. L., & Johnson, B. D. 2007, *ApJ*, 666, 34
- Madau, P., & Phinney, E. S. 1996, *ApJ*, 456, 124
- Madau, P., & Pozzetti, L. 2000, *MNRAS*, 312, L9
- Madau, P., Rees, M. J., Volonteri, M., Haardt, F., & Oh, S. P. 2004, *ApJ*, 604, 484
- MAGIC Collaboration. 2008, *Science*, 320, 1752
- MAGIC Collaboration et al. 2014, ArXiv e-prints
- Mankuzhiyil, N., Persic, M., & Tavecchio, F. 2010, *ApJ*, 715, L16
- Matsuoka, Y., Ienaka, N., Kawara, K., & Oyabu, S. 2011, *ApJ*, 736, 119
- Matsuura, S., et al. 2011, *ApJ*, 737, 2
- Mattila, K. 1990, in *IAU Symposium*, Vol. 139, *The Galactic and Extragalactic Background Radiation*, ed. S. Bowyer & C. Leinert, 257–268
- Maurer, A., Raue, M., Kneiske, T., Horns, D., Elsässer, D., & Hauschildt, P. H. 2012, *ApJ*, 745, 166
- Mazin, D., & Raue, M. 2007, *A&A*, 471, 439
- Meyer, M., Horns, D., & Raue, M. 2013, *Phys. Rev. D*, 87, 035027
- Meyer, M., Horns, D., & Zechlin, H.-S. 2010, *A&A*, 523, A2
- Meyer, M., Raue, M., Mazin, D., & Horns, D. 2012, *A&A*, 542, A59
- Muriel, H., Donzelli, C., Rovero, A. C., & Pichel, A. 2015, *A&A*, 574, A101
- Nikishov, A. I. 1962, *Soviet Physics JETP*, 14, 393
- Nolan, P. L., et al. 2012, *ApJS*, 199, 31
- Odegard, N., Arendt, R. G., Dwek, E., Haffner, L. M., Hauser, M. G., & Reynolds, R. J. 2007, *ApJ*, 667, 11
- Orr, M. R., Krennrich, F., & Dwek, E. 2011, *ApJ*, 733, 77
- Pénin, A., et al. 2012, *A&A*, 543, A123
- Perlman, E. S., Padovani, P., Giommi, P., Sambruna, R., Jones, L. R., Tzioumis, A., & Reynolds, J. 1998, *AJ*, 115, 1253
- Piron, F., & CAT Collab. 2000, in *American Institute of Physics Conference Series*, Vol. 515, *American Institute of Physics Conference Series*, ed. B. L. Dingus, M. H. Salamon, & D. B. Kieda, 113–118
- Piron, F., et al. 2001, *A&A*, 374, 895
- Pita, S., et al. 2014, *A&A*, 565, A12
- Planck Collaboration et al. 2014, *A&A*, 571, A1
- Prandini, E., Bonoli, G., Maraschi, L., Mariotti, M., & Tavecchio, F. 2011, arXiv:1101.4098
- Prandini, E., Bonoli, G., & Tavecchio, F. 2012, *A&A*, 543, A111
- Protheroe, R. J., & Meyer, H. 2000, *Physics Letters B*, 493, 1
- Raue, M., & Mazin, D. 2008, *International Journal of Modern Physics D*, 17, 1515
- Reimer, A. 2007, *ApJ*, 665, 1023
- Rubtsov, G. I., & Troitsky, S. V. 2014, *Soviet Journal of Experimental and Theoretical Physics Letters*, 100, 355
- Salamon, M. H., Stecker, F. W., & de Jager, O. C. 1994, *ApJ*, 423, L1
- Sanchez, D. A., Fegan, S., & Giebels, B. 2013, *A&A*, 554, A75
- Sánchez-Conde, M. A., Paneque, D., Bloom, E., Prada, F., & Domínguez, A. 2009, *Phys. Rev. D*, 79, 123511
- Schroeder, M., et al. 2005, *ApJ*, 634, 947
- Shao, L., & Ma, B.-Q. 2010, *Modern Physics Letters A*, 25, 3251
- Sharma, M., Nayak, J., Koul, M. K., Bose, S., Mitra, A., Dhar, V. K., Tickoo, A. K., & Koul, R. 2015, *Nuclear Instruments and Methods in Physics Research A*, 770, 42
- Sinha, A., Sahayanathan, S., Misra, R., Godambe, S., & Acharya, B. S. 2014, *ApJ*, 795, 91
- Stecker, F. W., de Jager, O. C., & Salamon, M. H. 1992, *ApJ*, 390, L49
- Stecker, F. W., & Glashow, S. L. 2001, *Astroparticle Physics*, 16, 97
- Stecker, F. W., Malkin, M. A., & Scully, S. T. 2006, *ApJ*, 648, 774
- . 2012, *ApJ*, 761, 128
- Tagliaferri, G., et al. 2008, *ApJ*, 679, 1029
- Tavecchio, F., Roncadelli, M., Galanti, G., & Bonoli, G. 2012, *Phys. Rev. D*, 86, 085036
- Teplitz, H. I., et al. 2011, *AJ*, 141, 1
- Totani, T., Yoshii, Y., Maihara, T., Iwamuro, F., & Motohara, K. 2001, *ApJ*, 559, 592
- Vasileiou, V., et al. 2013, *Phys. Rev. D*, 87, 122001
- Xu, C. K., et al. 2005, *ApJ*, 619, L11
- Yang, J., & Wang, J. 2010, arXiv:1006.4401
- Zemcov, M., Blain, A., Halpern, M., & Levenson, L. 2010, *ApJ*, 721, 424
- Zemcov, M., et al. 2014, *Science*, 346, 732
- Zhou, Y., Yan, D., Dai, B., & Zhang, L. 2014, *PASJ*, 66, 12

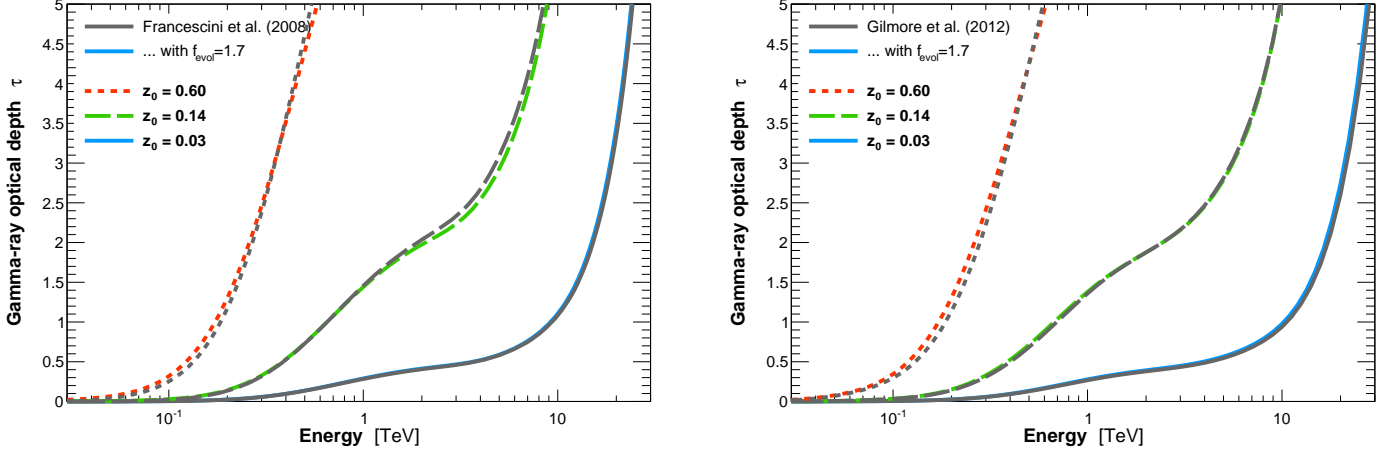


FIG. 11.— Attenuation curves for three different redshifts, from $z = 0.03$ up to $z = 0.6$. Gray curves are directly extracted from the publications of Franceschini et al. (2008) (*left*) and Gilmore et al. (2012) (*right*). Colored curves are based on the same $z = 0$ EBL density as in the publications but assume a template EBL evolution with $f_{\text{evol}} = 1.7$.

APPENDIX

A. SYSTEMATIC UNCERTAINTIES

We discuss in Sec. A.1 and Sec. A.2 the approximations to the spectrum and evolution of the EBL used in this paper. We estimate in Sec. A.3 the systematic uncertainty arising from these approximations as well as those coming from the modeling of the intrinsic spectra and the possible biases in the energy scale.

A.1. EBL evolution

We compare, in Fig. 11, gamma-ray optical depths published by Franceschini et al. (2008) and Gilmore et al. (2012) with optical depths derived from Eq. 9, assuming the $z = 0$ specific intensities as given in each paper with a template evolution with $f_{\text{evol}} = 1.7$. The published attenuation curves and those derived from Eq. 9 are in very good agreement, which supports the analytical approach in Sec. 2. The differences between published and template optical depths, $\Delta\tau$, are shown in Fig. 12. The value of $f_{\text{evol}} = 1.7$ is adopted (intermediate panels) and can be compared to softer and harder evolution in the bottom and top panels, respectively. We note that the evolution used by Raue & Mazin (2008), $f_{\text{evol}} = 1.2$, results in significant deviations at large redshifts with respect to the models. Similarly, the published optical depths are underestimated by the template approach at large redshifts for a soft evolution with $f_{\text{evol}} = 2.2$.

The template evolution with $f_{\text{evol}} = 1.7$ results in an optical depth difference on the order of 0.1 on average, which is comparable with the difference in evolution between the models of Franceschini et al. (2008) and Gilmore et al. (2012) themselves. As far as EBL evolution is concerned, assuming an energy-redshift decoupling in the local universe has then a similar impact on the absorption to using one or another state-of-the-art model.

Below an optical depth of 3, the deviation in the absorption factor remains smaller than 15%, which is below the typical systematic errors on gamma-ray fluxes measured by current-generation ground-based instruments. Another reference point for the difference in optical depth can be provided noting that a 5% deviation in H_0 , roughly the difference between $H_0 = 70 \text{ km s}^{-1} \text{ Mpc}^{-1}$ and the best-fit value from Planck Collaboration et al. (2014), results in a 5% deviation in optical depth, which corresponds to $\Delta\tau = 0.15$ (15% error on the absorption) for $\tau = 3$. Thus the template approach that we use in this publication introduces errors in the EBL no larger than those resulting from the uncertainties on H_0 or from the differences between state-of-the-art models.

For reference, the integrations in Eq. 9 and Eq. 10, which enable the computation of the optical depth, are performed using the trapezoidal rule, with uniform steps in redshift of $\delta z = 10^{-3}$ and in logarithmic reduced photon energy, $\delta e_0 = 5 \times 10^{-3}$, from the threshold of the EBL kernel, $e_0 = -2 \ln(1 + z_0)$, up to $e_0 = 10^3$. We checked that above $e_0 > 10^3$ the tail of the kernel in Fig. 1 has a negligible contribution to the convolution product in Eq. 9. The overall uncertainty on the optical depth $\tau(E_0, z_0)$ due to the numerical integration is on the order of 0.01-0.03, mildly depending on the redshift of the gamma-ray source.

A.2. Gaussian-sum approximation

Besides the evolution of the EBL, our second source of systematic error comes from the approximation of the true spectrum of the EBL by a sum of Gaussians, as in Eq. 17. We show in Fig. 13 the approximation of a “smooth” model $\nu I_\nu(\lambda)$, namely a sum of two log parabolas, by a Gaussian sum for a binning $\Delta_l = 0.75$, between $0.26 - 105 \mu\text{m}$, as in Sec. 3 and 4. The weights of the Gaussian-sum model are obtained by numerically inverting Eq. 20, where we set $\nu I_\nu^i = \nu I_\nu(\lambda_i)$.

The EBL kernel in Eq. 9 smooths the EBL density over a wide range of EBL wavelengths. The small deviations in intensity arising from the Gaussian-sum approximation then result in even milder optical-depth deviations, typically

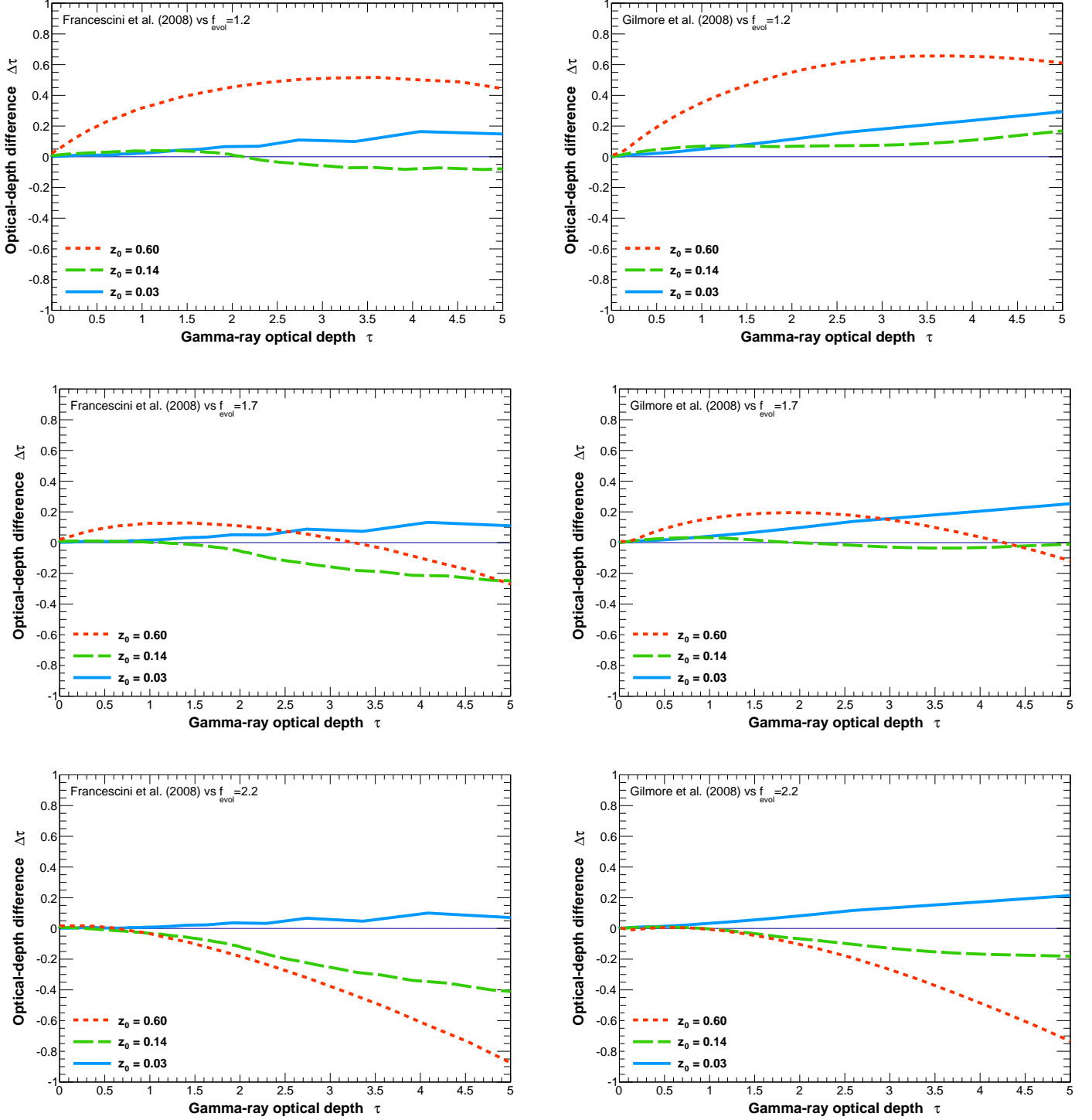


FIG. 12.— *Left:* Difference between optical depths obtained with a template evolution and with the model published by Franceschini et al. (2008). *Right:* Difference between optical depths obtained with a template evolution and with the model published by Gilmore et al. (2012). From *top to bottom*, the evolution parameter is $f_{\text{evol}} = 1.2$, $f_{\text{evol}} = 1.7$, and $f_{\text{evol}} = 2.2$. The intermediate evolution with $f_{\text{evol}} = 1.7$ is adopted.

$\delta\tau \leq 0.1, 0.01$, and 10^{-3} for $\Delta_l = 1.0, 0.5$, and 0.1 respectively.

A.3. Quantifying the systematic errors

To estimate the systematic uncertainties arising from the modeling of the EBL, i.e. from the template evolution and the Gaussian-sum approximation, we compare the optical depths derived by Franceschini et al. (2008) and Gilmore et al. (2012) to optical depths obtained with template evolution and approximating the Franceschini et al. (2008) or

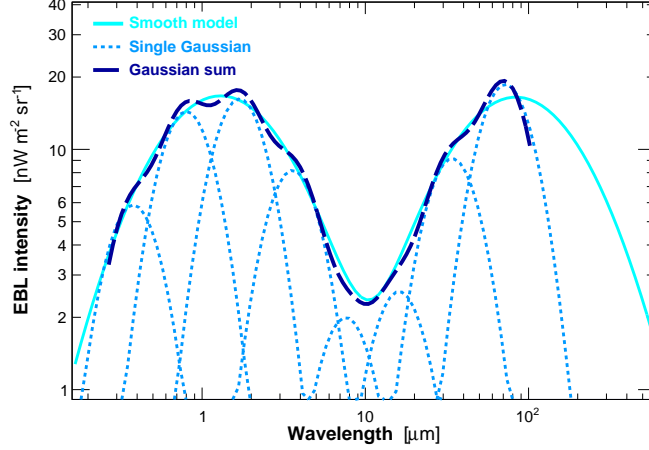


FIG. 13.— Smooth EBL intensity (sum of two log parabolas, solid cyan curve) approximated between $0.27 - 105 \mu\text{m}$ by a sum of Gaussians of width $\Delta_l = 0.75$ (dotted light blue). The resulting intensity is shown as a dark-blue dashed line.

Gilmore et al. (2012) SEDs at $z = 0$ by Gaussian sums.

We weight the contributions of the different optical depths based on the uncertainties on the spectral points included in the analysis. The measured optical depth depends on the measured flux, ϕ , as $\ln \phi = \ln \phi_{\text{int}} - \tau$, so that the maximum uncertainty on the optical depth, obtained by fixing the intrinsic model, scales as σ_ϕ / ϕ . Then, one can estimate the EBL normalization factor α that accounts for the change from the model, of optical depth τ_{model} , to the template approach, of optical depth τ_{template} , by minimizing:

$$\chi^2(\alpha) = \sum \frac{(\tau_{\text{template},i} - \alpha \times \tau_{\text{model},i})^2}{(\sigma_{\phi,i} / \phi_i)^2} \quad (\text{A1})$$

which gives

$$\alpha = \frac{\sum \tau_{\text{model},i} \tau_{\text{template},i} \times (\phi_i / \sigma_{\phi,i})^2}{\sum \tau_{\text{model},i}^2 \times (\phi_i / \sigma_{\phi,i})^2} \quad (\text{A2})$$

Since the optical depth is proportional to the EBL intensity and inversely proportional to the Hubble constant, the systematic relative bias of the optical depth, $\alpha - 1$, contributes equally the systematic uncertainty of the EBL intensity and Hubble constant. Using the gamma-ray cosmology sample, and assuming a binning of $\Delta_l = 0.75$, we find an average bias of 0.5 % for the model of Franceschini et al. (2008) and 1.8 % for the model of Gilmore et al. (2012).

TABLE 5
SYSTEMATIC UNCERTAINTIES ON THE EBL SPECIFIC INTENSITY ESTIMATED
WITH TWO DIFFERENT MODELS.

	Franceschini et al. (2008)	Gilmore et al. (2012)
EBL modeling	0.5 %	1.8 %
Intrinsic model	2.3 %	5.2 %
Energy scale	6.2 %	6.0 %
Total	6.6 %	8.1 %

This source of systematic uncertainty is compared with the two other principal sources that have been identified: the gamma-ray energy scale and the choice of intrinsic model for each spectrum. The EBL scaling factor of the models of Franceschini et al. (2008) and Gilmore et al. (2012) are estimated as in Sec. 4.1, additionally shifting the energy scale of the Cherenkov experiment within $\pm 10\%$ on one hand, and using exclusively log-parabolas or exponential cut-off power laws for the intrinsic spectra on the other hand. A systematic energy bias of $\pm 10\%$ is a conservative estimate with respect to the value half as large found in Meyer et al. (2010) by studying the marginal mismatch between HE and VHE observations of the Crab nebula, but is comparable to the systematic error typically quoted by the observers. The energy scale impacts the EBL intensity at the $\sim 6\%$ level. Changing the gamma-ray spectral models impacts the EBL normalization at the 2 – 5 % level. The total systematic uncertainty on the EBL flux level and on the Hubble constant are estimated in Table 5 by summing in quadrature the various sources of systematic errors to be about 7 – 8 %.

We also estimate the systematic bias on the flux enhancement discussed in Sec. 4.4. Using the full sample, we compute the average flux bias, FB , as the flux enhancement resulting from using the template approach instead of

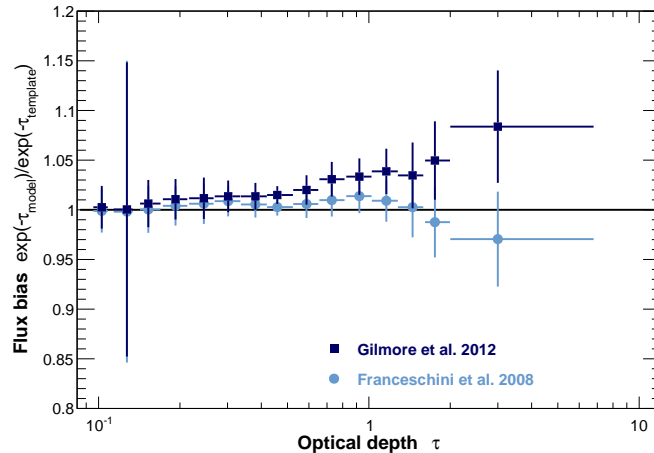


FIG. 14.— Ratio of gamma-ray attenuation from the model of Franceschini et al. (2008) (light blue circles) and Gilmore et al. (2012) (dark blue squares) to the value obtained with our templates, using the full sample of gamma-ray spectra.

the model:

$$FB = \exp[(\alpha - 1) \times \tau_{\text{model}}] \quad (\text{A3})$$

where α is computed as in Eq. A2. The flux bias is shown as a function of optical depth in Fig. 14, for the full sample. Using the gamma-ray cosmology sample yields similar average values for each of the two models, though with a rather constant behavior across the whole optical depth range. An underestimation of the absorption of about 10 % at optical depth $\tau > 2$ is visible in Fig. 14 for the model of Gilmore et al. (2012), although the large uncertainties do not allow a firm conclusion. For the sake of argument, we consider 10 % as the systematic uncertainty on the flux enhancement at large optical depths. Improved statistics will result in a more accurate estimate of this systematic uncertainty in the future.

B. BEST-FIT PARAMETERS AND COVARIANCE MATRICES

In the following, we describe the best-fit EBL spectrum derived using gamma-ray data only (4 parameters) and gamma-ray data together with local constraints (8 parameters). The EBL intensities and associated uncertainties in each wavelength bin can be computed from Eq. 20. The best-fit parameters of the gamma-ray data only are shown in Table 6, with covariance matrix shown in Table 7. The best-fit parameters and covariance matrix for the gamma-ray data and local constraints are shown in Tables 8 and 9. The optical depths derived with the eight-point spectrum between 50 GeV and 20 TeV are shown in Tables 10 and 11. We limit the results to optical depths less than 5, where we have good control of the systematic errors, as discussed in Appendix A.

TABLE 6
PARAMETERS OF THE BEST-FIT EBL SPECTRUM
USING GAMMA-RAY DATA ONLY.

λ μm	a_i $\text{nW m}^{-2} \text{sr}^{-1}$
0.55	18.1
2.47	8.05
11.1	0.91
49.7	4.51

TABLE 7
COVARIANCE MATRIX OF THE BEST-FIT EBL PARAMETERS USING GAMMA-RAY
DATA ONLY.

1	2	3	4
18.66	4.58	1.62	0.38
...	1.83	0.52	0.17
...	...	0.35	0.04
...	0.21

TABLE 8
PARAMETERS OF THE BEST-FIT EBL SPECTRUM USING GAMMA-RAY DATA AND
LOCAL CONSTRAINTS.

λ μm	a_i $\text{nW m}^{-2} \text{sr}^{-1}$
0.38	7.12
0.80	12.6
1.70	10.3
3.60	6.79
7.62	-0.61
16.1	4.56
34.1	1.30
72.3	11.9

TABLE 9
COVARIANCE MATRIX OF THE BEST-FIT EBL PARAMETERS USING GAMMA-RAY
DATA AND LOCAL CONSTRAINTS.

1	2	3	4	5	6	7	8
21.710	-3.450	0.659	-0.001	-0.054	-0.007	-0.006	-0.020
...	6.153	-0.435	1.244	0.076	0.076	-0.001	0.019
...	...	0.802	-0.108	0.232	-0.004	0.012	0.031
...	0.827	-0.069	0.066	-0.008	0.004
...	0.434	-0.035	0.032	0.052
...	0.109	-0.030	0.051
...	0.081	-0.084
...	1.743

TABLE 10
OPTICAL DEPTH BETWEEN 50 GeV AND 20 TeV FOR SOURCES AT REDSHIFT
BETWEEN 0.01 AND 0.31.

TeV / z	0.01	0.03	0.05	0.07	0.09	0.11	0.13	0.15	0.17	0.19	0.21	0.23	0.25	0.27	0.29	0.31
0.050	0.00	0.00	0.00	0.00	0.00	0.00	0.00	0.00	0.00	0.00	0.00	0.01	0.01	0.01	0.01	0.01
0.061	0.00	0.00	0.00	0.00	0.00	0.00	0.00	0.01	0.01	0.01	0.01	0.01	0.02	0.02	0.02	0.03
0.075	0.00	0.00	0.00	0.01	0.01	0.01	0.01	0.02	0.02	0.02	0.03	0.03	0.04	0.05	0.05	0.06
0.091	0.00	0.00	0.01	0.01	0.02	0.02	0.03	0.04	0.04	0.05	0.06	0.07	0.08	0.09	0.10	0.12
0.111	0.00	0.01	0.02	0.02	0.03	0.04	0.05	0.07	0.08	0.09	0.11	0.12	0.14	0.16	0.18	0.20
0.136	0.01	0.02	0.03	0.04	0.06	0.07	0.09	0.11	0.13	0.15	0.18	0.20	0.23	0.26	0.29	0.32
0.166	0.01	0.03	0.05	0.07	0.09	0.12	0.14	0.17	0.21	0.24	0.27	0.31	0.35	0.39	0.44	0.48
0.202	0.01	0.04	0.07	0.11	0.14	0.18	0.22	0.26	0.31	0.36	0.41	0.46	0.51	0.57	0.63	0.69
0.247	0.02	0.06	0.11	0.15	0.21	0.26	0.32	0.37	0.44	0.50	0.57	0.64	0.71	0.79	0.87	0.95
0.302	0.03	0.09	0.15	0.21	0.28	0.35	0.43	0.51	0.59	0.68	0.76	0.86	0.95	1.05	1.15	1.25
0.368	0.04	0.12	0.20	0.28	0.37	0.47	0.57	0.67	0.77	0.88	0.99	1.11	1.23	1.35	1.48	1.61
0.450	0.05	0.15	0.26	0.37	0.48	0.60	0.72	0.85	0.98	1.11	1.25	1.40	1.54	1.69	1.84	2.00
0.549	0.06	0.19	0.32	0.46	0.60	0.74	0.90	1.05	1.21	1.37	1.54	1.71	1.88	2.06	2.24	2.43
0.671	0.08	0.23	0.39	0.56	0.73	0.90	1.08	1.27	1.46	1.65	1.85	2.05	2.25	2.46	2.67	2.88
0.819	0.09	0.28	0.47	0.66	0.86	1.07	1.28	1.50	1.72	1.94	2.17	2.40	2.63	2.87	3.11	3.35
1.00	0.11	0.32	0.55	0.77	1.01	1.24	1.48	1.73	1.98	2.23	2.48	2.73	2.99	3.25	3.51	3.77
1.22	0.12	0.37	0.62	0.88	1.14	1.40	1.66	1.93	2.20	2.47	2.74	3.01	3.28	3.55	3.82	4.08
1.49	0.13	0.41	0.68	0.96	1.23	1.51	1.79	2.07	2.35	2.63	2.90	3.18	3.45	3.72	4.00	4.27
1.82	0.14	0.43	0.71	1.00	1.28	1.57	1.85	2.13	2.41	2.69	2.97	3.25	3.52	3.80	4.07	4.34
2.22	0.14	0.43	0.72	1.01	1.30	1.58	1.87	2.15	2.43	2.72	3.00	3.29	3.57	3.86	4.15	4.44
2.71	0.15	0.44	0.73	1.02	1.31	1.60	1.90	2.19	2.49	2.80	3.11	3.42	3.73	4.06	4.38	4.72
3.31	0.15	0.45	0.76	1.07	1.38	1.70	2.03	2.36	2.70	3.05	3.41	3.77	4.14	4.52	4.91	...
4.05	0.17	0.50	0.85	1.20	1.56	1.93	2.32	2.71	3.11	3.52	3.95	4.38	4.82
4.94	0.19	0.59	0.99	1.41	1.84	2.29	2.74	3.21	3.69	4.18	4.68

TABLE 10 — *Continued*

TeV / z	0.01	0.03	0.05	0.07	0.09	0.11	0.13	0.15	0.17	0.19	0.21	0.23	0.25	0.27	0.29	0.31
6.03	0.23	0.70	1.18	1.68	2.19	2.71	3.25	3.80	4.36	4.94
7.37	0.27	0.82	1.39	1.98	2.57	3.19	3.82	4.46
9.00	0.32	0.97	1.63	2.32	3.03	3.77	4.53
11.0	0.38	1.17	2.00	2.86	3.77	4.73
13.4	0.50	1.56	2.69	3.89
16.4	0.73	2.29	3.98
20.0	1.11	3.46

TABLE 11
OPTICAL DEPTH BETWEEN 50 GeV AND 6 TeV FOR SOURCES AT REDSHIFT
BETWEEN 0.33 AND 0.61.

TeV / z	0.33	0.35	0.37	0.39	0.41	0.43	0.45	0.47	0.49	0.51	0.53	0.55	0.57	0.59	0.61
0.050	0.01	0.02	0.02	0.02	0.02	0.03	0.03	0.04	0.04	0.05	0.05	0.06	0.06	0.07	0.08
0.061	0.03	0.04	0.04	0.05	0.06	0.06	0.07	0.08	0.09	0.10	0.11	0.12	0.13	0.14	0.15
0.075	0.07	0.08	0.09	0.10	0.11	0.12	0.13	0.15	0.16	0.18	0.19	0.21	0.23	0.24	0.26
0.091	0.13	0.14	0.16	0.18	0.20	0.21	0.23	0.26	0.28	0.30	0.33	0.35	0.38	0.41	0.43
0.111	0.22	0.24	0.27	0.29	0.32	0.35	0.38	0.41	0.45	0.48	0.52	0.55	0.59	0.63	0.68
0.136	0.35	0.39	0.42	0.46	0.50	0.54	0.59	0.63	0.68	0.73	0.78	0.83	0.88	0.94	0.99
0.166	0.53	0.58	0.63	0.68	0.74	0.80	0.85	0.92	0.98	1.04	1.11	1.18	1.25	1.32	1.40
0.202	0.76	0.82	0.89	0.96	1.04	1.11	1.19	1.27	1.35	1.44	1.52	1.61	1.70	1.80	1.89
0.247	1.03	1.12	1.21	1.30	1.40	1.49	1.59	1.70	1.80	1.91	2.02	2.13	2.24	2.36	2.47
0.302	1.36	1.47	1.58	1.70	1.82	1.94	2.06	2.19	2.32	2.45	2.58	2.72	2.86	3.00	3.14
0.368	1.74	1.87	2.01	2.15	2.30	2.45	2.60	2.75	2.90	3.06	3.22	3.38	3.54	3.71	3.88
0.450	2.16	2.32	2.49	2.66	2.83	3.00	3.18	3.36	3.54	3.73	3.91	4.10	4.29	4.48	4.68
0.549	2.62	2.81	3.00	3.20	3.40	3.60	3.81	4.02	4.23	4.44	4.65	4.86
0.671	3.10	3.32	3.55	3.77	4.00	4.22	4.45	4.69	4.92
0.819	3.59	3.83	4.08	4.32	4.57	4.82
1.00	4.03	4.29	4.54	4.80
1.22	4.35	4.62	4.88
1.49	4.53	4.80
1.82	4.62	4.89
2.22	4.73

C. INDIVIDUAL SPECTRA

The 106 VHE spectra studied in this paper are shown in Fig. 16-19. The publications from which these data are extracted can be found in Table 2. Observed VHE spectral points are shown in dark blue and the models best fitting these data are shown as a blue-gray solid line. The intrinsic spectral points are shown in light blue, after deabsorption with the best-fit EBL spectrum. The associated butterfly (one sigma envelope of the best-fit intrinsic model) is shown as a cyan contour. The butterflies associated with *Fermi*-LAT data are shown in dashed gray for non-contemporaneous HE and VHE observations, and in dashed black whenever the HE and VHE data are quasi-contemporaneous. The border of each spectral panel is colored as in Fig. 2, light blue indicating the gamma-ray cosmology sample, dark red the sources with under-constrained redshifts, and orange the FSRQs.

The contemporaneity criterion is rather loose, and the HE and VHE integration windows differ in duration, albeit having a temporal overlap. For this reason, some VHE spectra show a flux level slightly larger than their quasi-contemporaneous counterpart (2 of 33) while some show a somewhat smaller flux level (4 of 33). No conclusion can be drawn from these mild discrepancies given the astrophysical uncertainties in the mechanism responsible for the variability of blazars and the differences between the HE and VHE exposures.

The constraints from the hardness of the intrinsic spectra based on quasi-contemporaneous HE observations (see Eq. 13) seem *a posteriori* rather weak. Nine spectra show non-zero χ^2 contributions, the most important one being obtained for **Mkn501_ARG0-YBJ_flare2011**, with $\chi^2_{\text{HE-VHE}} = 3.3 \times 10^{-2}$. The remaining eight show χ^2 values smaller than 10^{-2} .

The distribution of the intrinsic photon indices is shown in Fig. 15. For the spectra described by log parabolas and exponential cut-off power laws, the indices are computed at the decorrelation energy. The minimum indices are $\Gamma = 1.35 \pm 0.24$ and $\Gamma = 1.37 \pm 0.30$, obtained for **Mkn421_MAGIC_2006-04-27** and **H1426+428_HEGRA_2002** respectively, indicating that all of these spectra are compatible with the maximum hardness, $\Gamma > 1.5$, expected within a standard synchrotron self-Compton model for an electron index of 2.

All the spectra show good fits, with 103 of them having χ^2 probabilities larger than 15 %. The three poorest fits are **PKS0301-243_HESS_2009-2010**, **Mkn501_ARG0-YBJ_flare2011**, and **Mkn421_VERITAS_2008_highB** with χ^2 probabilities of 9 %, 14 %, and 14 % respectively.

Finally, we would like to stress a natural bias arising from the visual scanning of these spectra. It appears that some VHE spectra show important upward going fluctuations with respect to their best-fit model, see e.g. the last

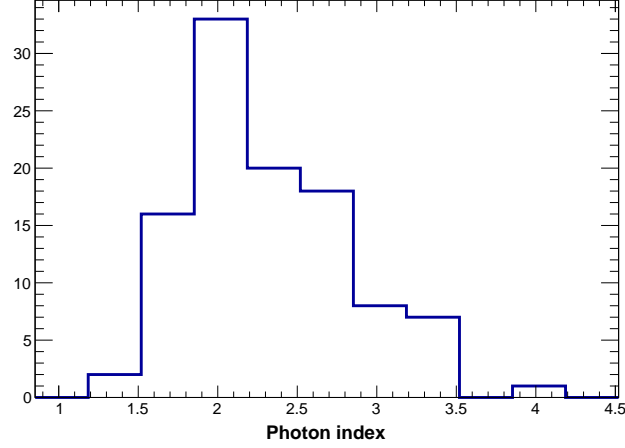


FIG. 15.— Distribution of the intrinsic photon indices.

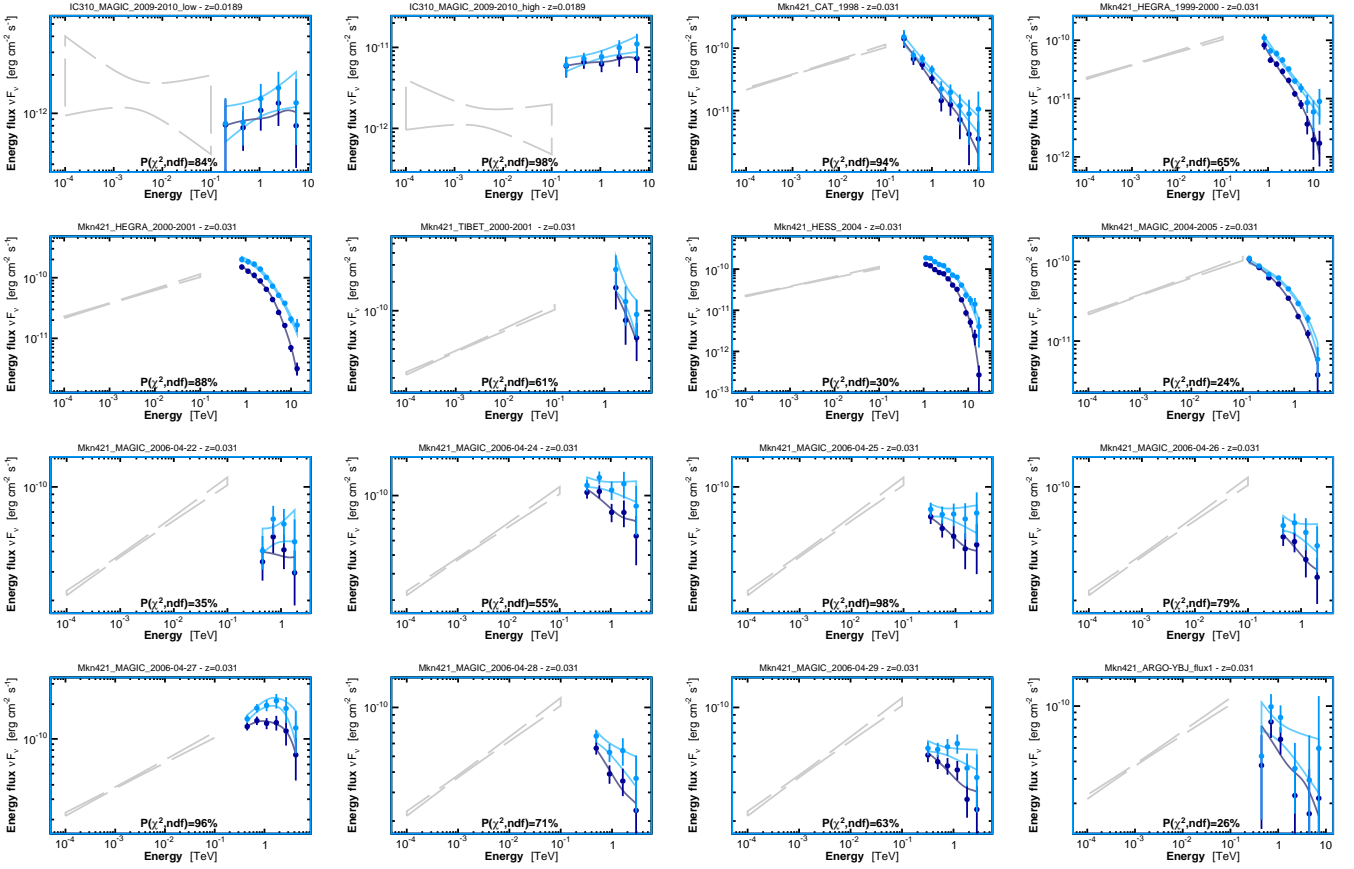


FIG. 16.— Best-fit spectra 1 of 4. See text for more details.

spectral points of Mkn421_ARGO-YBJ_flux3 and 1ES0229+200_HESS_2005-2006. These cases are particularly striking to the eye with flux enhancements of ~ 1600 and ~ 23 , respectively. In practice, such deviations are of rather small amplitude when normalized to the uncertainty on the flux, with deviations of only 1.2σ and 1.3σ for these two examples. The logarithmic scale of the plot is of course responsible for the visual bias that artificially amplifies upward going fluctuations.

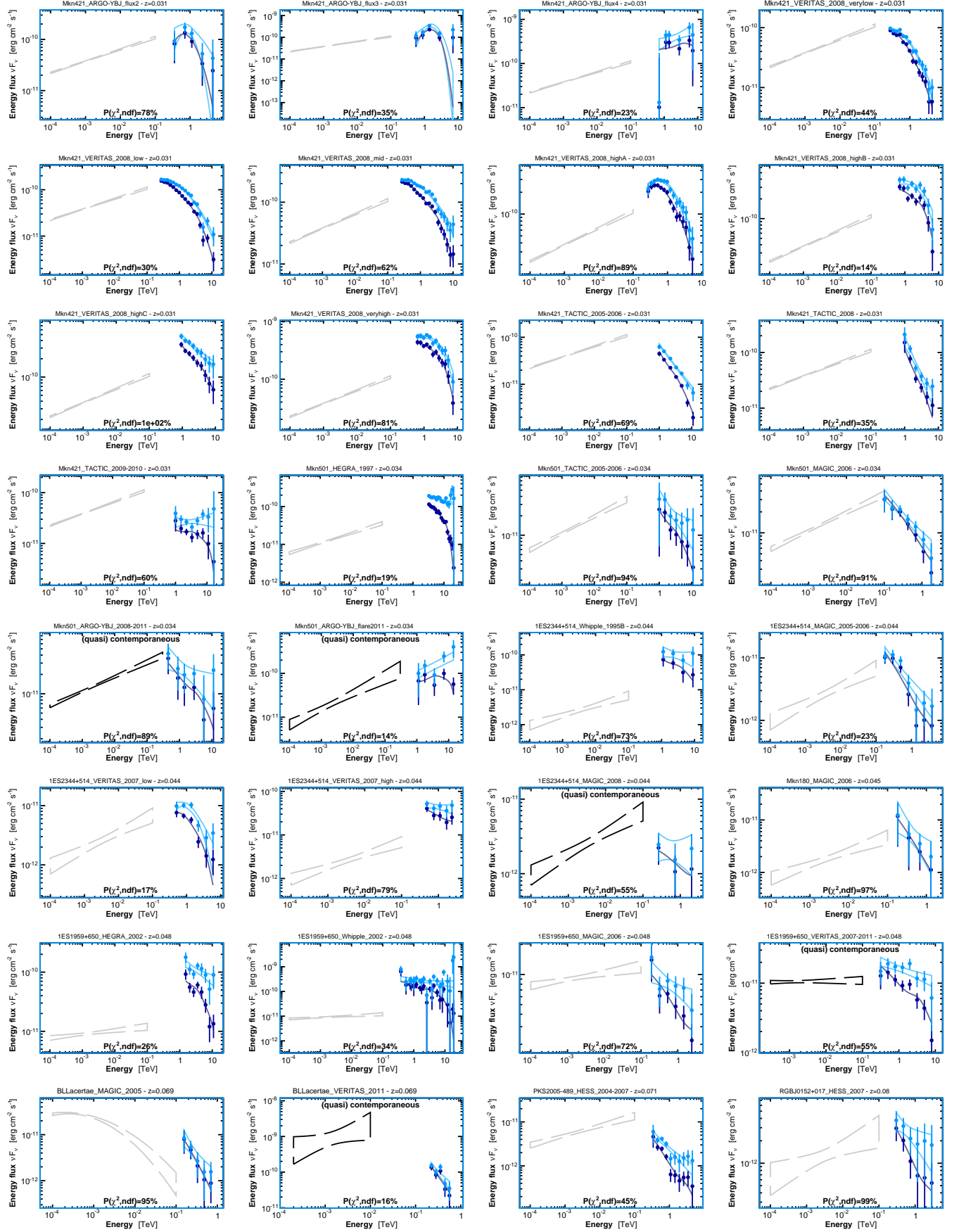


FIG. 17.— Best-fit spectra 2 of 4. See text for more details.

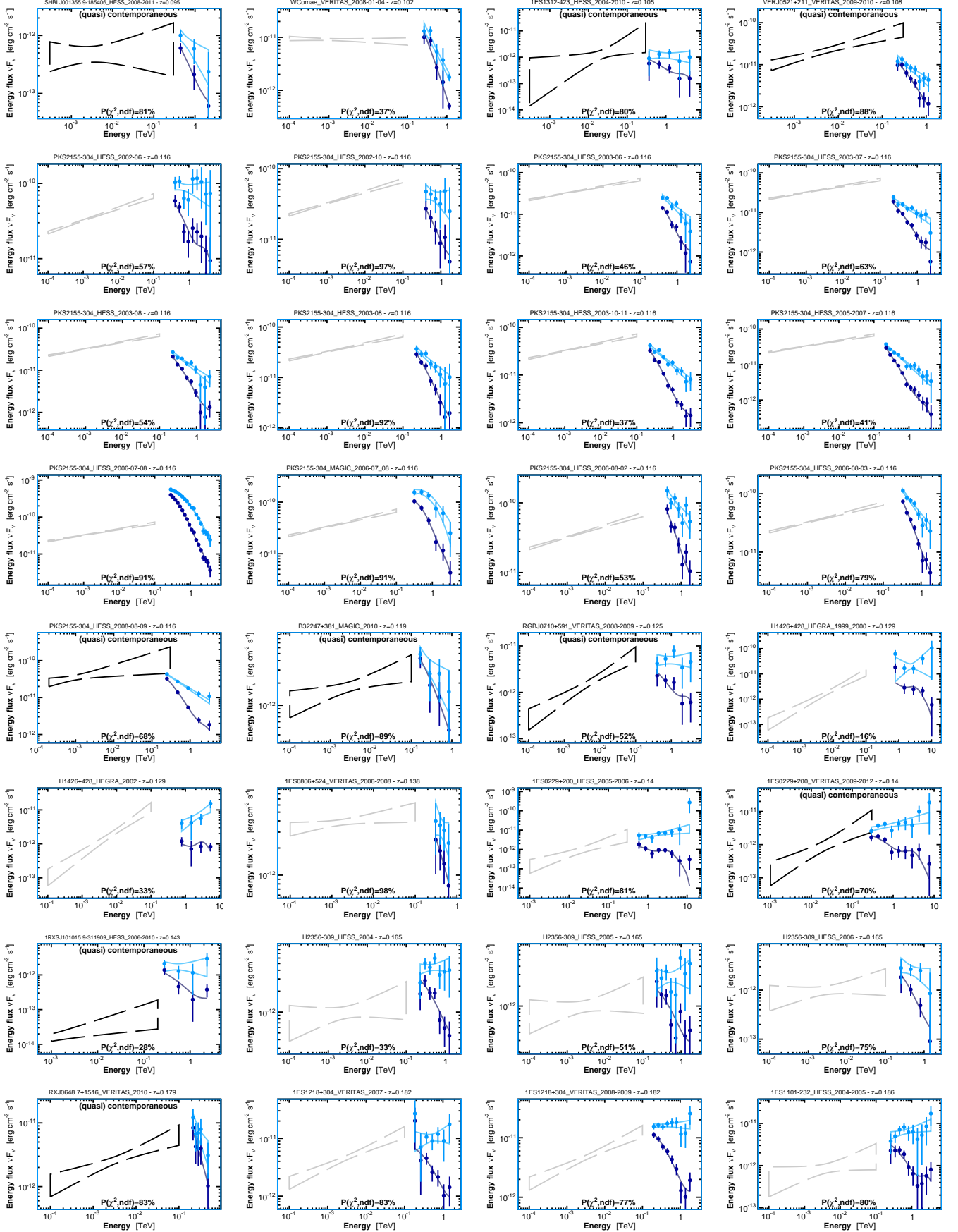


FIG. 18.— Best-fit spectra 3 of 4. See text for more details.

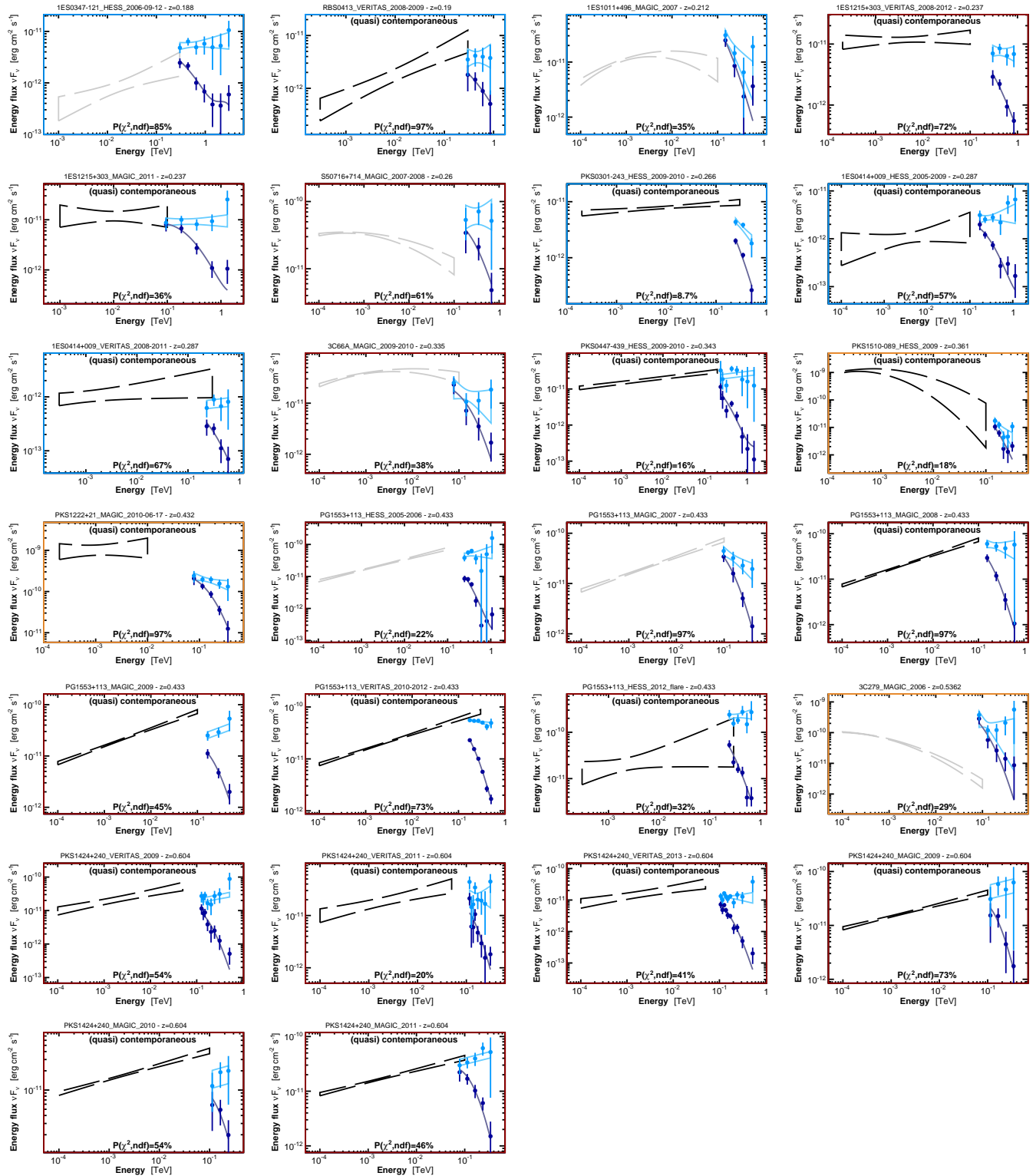


FIG. 19.— Best-fit spectra 4 of 4. See text for more details.